POST-VARISCAN MAFIC DIKES FROM THE LATE OROGENIC COLLAPSE TO THE TETHYAN RIFT: EVIDENCE FROM SARDINIA

Laura Gaggero*,✉, Giacomo Oggiano, Laura Buzzi*, Francesca Slejko***** and **Luciano Cortesogno***†

***** *Dipteris., Università di Genova, Corso Europa 26, I-16132 Genova, Italy.*
****** *Istituto di Scienze Geologico - Mineralogiche, Università di Sassari, Corso Angjoi 10, Sassari, I- 07100, Italy.*
******* *Dipartimento di Scienze della Terra, Via Weiss 8, I- 34127 Trieste, Italy.*
✉ *Corresponding author, e-mail: gaggero@dipteris.unige.it.*

Keywords: *transitional basalts, $^{40}Ar/^{39}Ar$ geochronology, Sr-Nd systematics, lithospheric extension, mantle, Permo-Triassic. Sardinia.*

ABSTRACT

Dolerite dikes cut the Lower Paleozoic medium- to high-grade metamorphic basement, the Sardinia-Corsica batholith and the Stephanian - Autunian calc-alkaline effusives (1st volcanic episode, according e.g. to Bonin, 1989; Cabanis et al., 1990) with a N-S trend and subvertical dip. Their occurrence is reported from several areas of Sardinia, from the N to the SE. The basic dikes are associated with diorite to rhyolite dikes having trends ranging from E-W to N-S. A late Triassic lamprophyric dike intruded the garnet-staurolite-kyanite micaschists near Mt. Nieddu and has a 40°N direction. Two ^{40}Ar-^{39}Ar age determinations for the dolerite dikes were carried out on amphibole. Ages between 253.8±4.9 and 248±8 Ma (Permian - Early Triassic) probably correspond to the emplacement interval.

A continental within-plate geochemical signature, with prevalent tholeiitic to transitional (dolerites) and minor alkalic (lamprophyre) terms, has been determined. The relative LILE and REE enrichment compared with the MORBs and Nd isotopic ratios (4 bulk samples; initial $^{143}Nd/^{144}Nd$ ratios between 0.512529±0.000025 and 0.513143±0.000023) is consistent with a source in a sub-continental lithospheric mantle. The remarkable compositional and isotopic variability can be explained by the partial melting of a heterogeneous source. Crustal contamination variably affects some transitional dikes; the host Arzachena monzogranite probably represents the major contaminant source.

On the whole, the geochemical data support an anorogenic geochemical affinity, in accordance with the extensional regional tectonics, for the Permo-Triassic dikes in Sardinia. The E-W emplacement patterns correspond to the major fractures and primarily R and RI structures associated with the late Variscan transcurrent-extensional E-W faults. The N-S emplacement trend is consistently associated with a generalized E-W extension of the Sardinian crust: in a pre-drift restoration it coincides with the patterns of extension between the European and Insubric crust at the beginning of the Tethyan rift.

In Sardinia, the lamprophyre dike is significantly younger than the late Variscan alkaline volcanites and dikes of the rest of the Mediterranean domain (e.g. Eastern Provence: 278-264 Ma, $^{40}Ar/^{39}Ar$ isotope dating on feldspar from rhyolites and on plagioclase from mafic flow, Zheng et al., 1992; Western Pyrenean Axial Zone: 271-266 Ma, K-Ar isotope dating on kaersutite phenocrysts from mafic dikes, Debon and Zimmermann, 1993), in accordance with the diachronism of both the first and second volcanic episodes in different areas of the Mediterranean domain. The overlap between the calc-alkaline events and the volcanic and sub-volcanic alkalic event, is not exclusive to Sardinia and Corsica (e.g. the Pyrenees and Pan-African orogen).

INTRODUCTION

The most recent geodynamic reconstructions of the late- and post- Variscan orogenic evolution of Southern Europe (Ziegler et al., 2001; Ziegler and Stampfli, 2001) are based on the integration of stratigraphic, paleontological, petrologic and geochemical datasets. In particular, the Carboniferous-Permian boundary (Gradstein et al., 2004) is characterized by the following large-scale events:

i) Crustal accretion, through conspicuous acidic intrusions, e.g. the build up of the Sardinia-Corsica batholith whose southern section developed between 340 and 288 Ma (U/Pb ages on zircon, Cocherie et al., 2005). The calc-alkaline acidic magmatism in the Southalpine domain (Schaltegger and Brack, 2007; Rottura et al., 1997; Rivalenti et al., 1980, with references) has a genetic link with partial melting in the lower crust and lithospheric mantle (Sinigoi et al., 1995, Stähle et al., 2001 for the Ivrea Zone).

ii) Orogenic collapse and tectonic unroofing, associated with localized transpressive or transtensional tectonics, active at a European scale between the Late Carboniferous and the Early Permian. The genesis of intramontane basins, controlled by transtensile tectonic phases (Ligurian Briançonnais, Sardinia, Southalpine, Balkan Terrane, Provence, Central Morocco, Pyrenees, Corsica) is coeval with the deposition of volcano-sedimentary successions characterized by fluvial-lacustrine sedimentation and sub-intrusive acidic to effusive basic-intermediate volcanic activity. The “calc-alkaline” serial affinity, common to the igneous rocks of the volcanic sedimentary sequences, and the stratigraphic features, generally define a first tectonic-volcanic-sedimentary cycle, active from the Appalachian range to most of Southern Europe (Cassinis et al., 1996; Cortesogno et al., 1998; Ziegler et al., 2001). However, in Corsica calc-alkaline products have recently been dated as old as Visean-Namurian (Rossi et al., 2006).

iii) A metamorphic thermal event, characterized by high T/P, spread at European scale (Deroin and Bonin, 2003).

In the following Late Permian-Triassic time interval, a second igneous cycle was characterized by transitional to alkalic serial affinity dated between 280 and 245 Ma. The activity included both extrusive and intrusive rocks such as metaluminous and alkaline granites and has a Late Carboniferous - Early Permian age in Corsica (Cocherie et al., 2005). The effusive rocks are not only alkalic basalts and rhyolites, but also tholeiitic basalts and important volumes of transitional basalts, emplaced as flows and dikes within sedimentary sequences and generally assumed to be related to an anorogenic environment. The most relevant occurrences of alkalic volcanics are in Morocco (Argana Basin, the High Atlas, Aït Chayeb et al., 1998), Western Pyrenean Axial Zone (Debon and Zimmermann, 1993), Provence

(Maure Vieille, Lapierre et al., 1999) and, subordinately, they crop out in Southern Corsica and North-Eastern Sardinia (Traversa et al., 2003). The tholeiitic to transitional volcanics occur in Corsica (Scandola-Senino Series, Cabanis et al., 1990; Bonin et al., 1993), Sardinia (Cortesogno et al., 1998; Traversa et al., 2003), Southalpine (Cassinis et al., 2007), the Pyrenees (Anayet Basin, Leroy and Cabanis, 1993), Provence (Esterel, Agay and Toulon basins, Lapierre et al., 1999) and Central Western Carpathia (Dostal et al., 2003). However, the inference is based on a generalized lack of reliable isotopic ages (e.g, U-Pb on zircon). The coeval sediments are fluvial clastic reddened successions in Bundsandstein facies related to an extensional regional tectonic regime.

In this context, the change from a subduction related calc-alkaline affinity (active in the Southalpine until the Triassic, $^{40}Ar/^{39}Ar$ step heating on hornblende = 217 Ma; Cassinis et al., 2007) to transitional and alkalic has been associated with the reactivation of older tectonic lineaments through strike slip faults (Bonin, 1989). The surface evidence is consistent with geochemical inferences of deepening of the magmatic source to the asthenospheric mantle (Leroy and Cabanis, 1993). The evolution from the late- to post-Variscan setting has been outlined in the Corsica-Sardinia area as calc-alkaline, basaltic and rhyolitic dyke activity (Traversa et al., 2003 and references within). This feature corresponds to the switch from the collapse of the Variscan cordillera to the global plate reorganisation (Ziegler et al., 2001) that resulted in the rifting of the Alpine Tethys in the Late Triassic.

During the Late Triassic, effusive products with an intraplate alkalic basalt (IAB) composition occur in the Eastern Pyrenees, Aquitaine, Morocco, Brittany, Algeria (Curnelle and Cabanis, 1989 and references therein), Majorca (Navidad and Alvaro, 1985) and Ecrins Pelvoux (Pelvoux-Rochail succession) in the Alpidic external massifs (Vatin-Perignon and Lemoine, 1982). On the whole, the petrogenesis is related to lithospheric thinning associated to the North Atlantic and/or Tethyan rifting and spreading.

This study addresses the petrologic, geochemical and geochronologic features of basic dikes occurring across the Lower Paleozoic basement of Sardinia with relatively unconstrained field relationships. Our goal was to provide insights into the lithospheric evolution between the post-Variscan collapse and the Tethyan rift.

GEOLOGICAL SETTING

The structural pattern of the Variscan belt in Sardinia is given by: 1) an external anchimetamorphic zone characterized by folds and thrusts 2) a nappe zone equilibrated under greenschist facies, and represented by a pile of tectonic units with a south-west sense of transport; 3) an internal zone formed by metamorphic rocks equilibrated under medium-P amphibolite facies and a high-grade metamorphic complex. The medium grade complex is in contact with the high-grade, migmatite-bearing metamorphic complex through a mylonitic belt. The migmatitic complex includes eclogite relics of MORB affinity, whose protolith was dated at 457±2 Ma and the peak metamorphism at 403±4 Ma (Cortesogno et al., 2004), and accordingly interpreted as a Variscan suture (Cappelli et al., 1991; Carmignani et al., 1994).

The Lower Paleozoic polymetamorphic basement was intruded by the Sardinia-Corsica batholith between 340 Ma (northern Corsica, Paquette et al., 2003) and 287 Ma (U-Pb SHRIMP method on zircon from A-type granites, Cocherie et al., 2005). The syn- to post-collisional emplacement of the batholith occurred in a regional extensional regime (Oggiano, 1994; Cortesogno et al., 1998) associated with a high thermal flow. As a consequence of the isotherm perturbation at various places in northern Sardinia the basement shows a HT-LP overprint (sillimanite, cordierite, K-feldspar, andalusite) coeval with the extensional structures (age of metamorphic micas: 293-308 Ma; Macera et al., 1989) and to the development of epithermal antimonite mineralizations (Muñoz et al., 1992).

A Stephanian-Autunian volcanic-sedimentary-tectonic sequence of events directly affected the three zones (Cortesogno et al., 1998). In south-western Sardinia the Guardia Pisano basin developed at 297±5 Ma (Pittau et al., 2002). In southern and south-eastern Sardinia, several Permo-Carboniferous basins (Seui, Perdasdefogu, Escalaplano) developed as strike-slip or pull-apart basins infilled with fluvio-lacustrine or fluvio-palustrine sediments associated with effusive and sub-intrusive products. To the SE, the polymetamorphic basement hosted NE-SW trending, calc-alkaline rhyolite dike swarms (CARG sheet 549, Muravera). Afterwards, still during the Early Permian, a large area (Barbagia di Seui) was affected by an important explosive acid volcanism, widely occurring in Sardinia (Ogliastra, Nurra, Gallura, Iglesiente), probably associated with a later, well-developed extensional phase (Cassinis et al., 2003). Subsequently, the sedimentation in the basins was sutured by one or more regional unconformities. The tectonic evolution can thus be envisaged to have switched from a transtensional to an extensional regime.

Mafic tholeiitic intrusions, dated to 305-304 Ma in Corsica (U/Pb, dissolution, Paquette et al., 2003), coeval to younger than the main Sardo-Corsican batholith were ascribed to other sources than acid magmas (Poli and Tommasini, 1999). However, younger gabbroic intrusions have been dated to 285-280 Ma and andesite basalt extrusives to 291-288 Ma (U-Pb SHRIMP on zircon, Cocherie et al., 2005). In Corsica, the age of alkaline volcano-plutonic associations has been re-assessed at about 287±1.8 Ma with U-Pb geochronology (Cocherie et al., 2005). A polyphase igneous activity is reported by Traversa et al. (2003) in Corsica and Sardinia between the Carboniferous and the Early Permian.

The on-going subduction of Paleotethys lithosphere at a regional scale might suggest an arc-related origin to account for the calc-alkalic signature of this volcanism. However, this process is in contrast with the evidence that the remnants of the Cambro-Ordovician and Devonian-Dinantian lithospheric extension represent a localized oceanization (Bodinier et al., 1988; Briand et al., 1988; von Raumer et al., 1990; Ménot and Paquette, 1993). Furthermore, there is no evidence of Paleozoic calc-alkaline andesitic magmatism associated with active margin systems in the Alpine and Pyrenean areas.

The eclogitic event closest in time developed between Ordovician and Dinantian times (U-Pb radiometric ages: 408-433 Ma, Gebauer et al., 1988; Paquette et al., 1989; Liégeois and Duchesne, 1981; Stenger et al., 1989; Bouchardon et al., 1989; Cortesogno et al., 1993; 1998), hardly supporting a direct genetic link between subduction and arc-related magmatism. A petrogenetic model for the Lower Permian magmatism, integrating the tectonic, petro-

logic and paleogeographic settings after the Pangea build-up, should assume (Cortesogno et al., 1998) a thick crustal pile created through a lower Ordovician-Dinantian underthrusting of the thinned Cambro-Ordovician crust and the subsequent stacking of crustal nappes (e.g. Carmignani et al., 1994). The orogen subsequently underwent isostatic re-equilibration, preceding its collapse, with consequent thermal uplift and metamorphic re-equilibration within the crust, dehydration reactions and crustal melting. At this moment, released fluids could have induced localized metasomatism of the underlying mantle. The subsequent collapse of the orogenic belt and the consequent adiabatic depressuring, recorded as eclogite-granulite transition at the lowest levels of the crustal pile, could have triggered melting processes in the lithospheric mantle and at the lower crust-mantle interface.

Therefore, conditions for the genesis of intermediate "calc-alkaline" liquids with a prevalent mantle and/or lower crust signature and acidic crustal melts (Green, 1982) could have occurred. Finally, their emplacement at shallow levels or at the surface would have been controlled by the extensional syn-collapse structures. The progressive development of an extensional, transtensional regime might have favored the ascent of magmas with a longer residence in the middle crust, and have made hybridization processes possible.

The evidence for a mid-Permian hiatus, marked by an unconformity throughout the Variscan segments in Europe, is provided by tectonic activity and high heat flow (Deroin and Bonin, 2003). In SW Sardinia, subvertical hydrothermal quartz dikes are aligned WNW-ESE across the basement (Cassinis et al., 2003) and likely postdate the development of the Seui basin.

A calc-alkaline dike event has been ascribed to partial melting of a lithospheric mantle source enriched in LILE and LREE by recycling of crustal material (Traversa and Vaccaro, 1992) possibly during earlier subduction events (Ronca et al., 1999). Traversa et al. (2003) consider the calc-alkaline event as related to orogenic activity, "although developing during a post-collisional extensional regime". The basaltic and transitional basaltic dikes have instead a crustal signature and are interpreted as clearly post-collisional and predating the Upper Permian rifting regime.

Fig. 1 - Schematic tectonic map of Sardinia. 1- Post-Variscan covers; 2- Late Variscan batholith; 3- High-grade metamorphic complex; 4- Internal nappes; 5- External nappes; 6- External zone; 7- Major and minor thrusts; 8- Posada-Asinara Line. Boxes: sampling areas.

Table 1 - GPS coordinates and locations of the studied samples.

LG101	COSTA SERENA	41°	11'	42.73"	9°	19'	56.73"
LG103	PORTO RAFAEL	41°	11'	41.35"	9°	20'	54.33"
LG19	CUPALCHIATA	41°	2'	20.71"	9°	23'	13.06"
LG60	PETRA NIEDDA	41°	9'	52.08"	9°	20'	56.33"
LG38	MIRIALVEDA	41°	4'	45.30"	9°	29'	25.74"
LG51	CONCA VERDE	41°	13'	13.50"	9°	16'	51.08"
LG53	CONCA VERDE	41°	13'	14.08"	9°	16'	50.07"
SG20	LI RENI	40°	54'	9.26"	8°	51'	8.60"
CPT1	MONTIGIU NIEDDU	40°	36'	14.78"	9°	35'	9.53"
FE12	CALANGIANUS - P.TA LU COLBU	40°	56'	10.70"	9°	12'	3.39"
FR38	M. E'SENES - BR.CU PILIERI	40°	27'	8.89"	9°	36'	8.93"
EB13	M. FERRU - GENNA E DIDU	39°	42'	26.87"	9°	39'	27.71"
EB7A	M. FERRU - ARCU DE SARRALA DESSUSU	39°	42'	5.00"	9°	38'	24.69"

Our investigation focuses on the dolerite dikes (Table 1) that cut the medium to high grade metamorphic basement (CARG sheet n. 411, Bocche di Bonifacio), the Variscan batholith (311+6/-4 Ma U/Pb on zircon, CARG sheet n. 428, Arzachena) and the calc-alkaline effusives of the 1st cycle (diorite dikes in the Artinskian Seui Basin; a dacite breccia in the Anglona region; rhyolitic ignimbrites at Montiferru di Tertenia; Fig. 1) with a N-S trend and subvertical dip. In southern Gallura, the dolerite dikes occur disrupted and partially assimilated within host monzogranites, thus constraining their early emplacement. The dolerite dikes range in composition from sub-alkalic to alkalic basalts; they are associated with diorite to rhyolite dikes with trends ranging from E-W to N-S: The E-W emplacement pattern is parallel to the major fractures and the primarily R and RI structures associated with late Variscan, transcurrent-extensional E-W faults. At Mt. Nieddu (Table 1), an alkaline basalt dike intruding garnet-staurolite-kyanite micaschists has a 40°N direction (Baldelli et al., 1987).

PETROGRAPHIC CHARACTERISTICS

Two dike compositions have been distinguished: 1) dolerites, the prevailing lithology, and 2) lamprophyre.

Dolerites

Meter-thick dolerites commonly show porphyritic (P.I. 2-15), and rarely glomeroporphyritic, seriate texture; the fine-medium to coarse-grained groundmass is intergranular/in-

tersertal to ophitic. Evident centimeter-thick chilled margins characterize the dikes, which locally exhibit phenocryst-(mostly plagioclase) preferred orientation. The phenocryst assemblage is represented by olivine, plagioclase and clinopyroxene. Phenocryst modal and grain size sorting (Ø 1.2 to 3.5 mm) is pronounced toward the core of some dikes (e.g. St. Pantaleo) as a result of flow differentiation.

Modal olivine attains about 15% in volume; olivine phenocrysts are diffusely replaced by chlorite ± actinolite ± tremolite. Very occasionally phenocrysts have lobated margins (Conca Verde) rimmed by granophyric aggregates of quartz and plagioclase, probably representing more or less advanced assimilation of quartzitic xenocrysts (Fig. 2A).

Generally well preserved euhedral plagioclase phenocrysts show normal zoning and frequent eutectic intergrowth with clinopyroxene. The occurrence of plagioclase megacrysts (about 5 mm) with lobate boundaries, suggests their possible exotic origin.

Chlorite + magnetite epitactic pseudomorphs on orthopyroxene occur as patches and probably represent the result of the following reaction series: 1) precipitation of a clinopyroxene + biotite phenocrystic assemblage, 2) replacement by hornblende, 3) dehydration of hornblende and its breakdown to orthopyroxene + magnetite + K-feldspar, 4) K-feldspar dissolution in the residual silicate melt, 5) chloritization of orthopyroxene (Fig. 2B). Orthopyroxene also occurs very occasionally as exsolution lamellae in clinopyroxene.

Euhedral to subhedral (Fig. 2C) and poikilitic clinopyroxene phenocrysts frequently show concentric zoning (Table 2). The poikilitic clinopyroxene can include biotite, K-feldspar and olivine. Hornblende overgrowths on clinopyroxene are widespread (Fig. 2D), suggesting volatile enrichment in the liquid before the shallow-level emplacement.

Euhedral to skeletal ilmenite shows eutectic precipitation with olivine and clinopyroxene. Ilmenite also occurs with titano-magnetite in trellis textures as products of oxidation and exsolution.

The groundmass is characterized by intergranular/intersertal to ophitic texture with a variable modal concentration of plagioclase, olivine, clinopyroxene, hornblende and ilmenite. Euhedral zoned plagioclase is the predominant phase; sometimes albite-K-feldspar intergrowths precipitate interstitially. Subhedral to skeletal clinopyroxene, subhedral and interstitial to poikilitic hornblende, ilmenite and interstitial glass represent the groundmass; subordinate pseudomorphosed olivine and rare spherulitic plagioclase also occur.

Needle-shaped to whisker apatite (0.2-1 mm) is a common accessory phase, reaching up to 1% in the groundmass. Sulfides and zircon are diffuse accessory phases.

Frequently, secondary alterations occur at the dike margins or are restricted to fractures. Alteration features have mostly developed under greenschist to subgreenschist facies conditions; 1) clinopyroxene can be overgrown by chlorite ± titanites ± clinozoisite ± tremolite and/or actinolite, 2) the

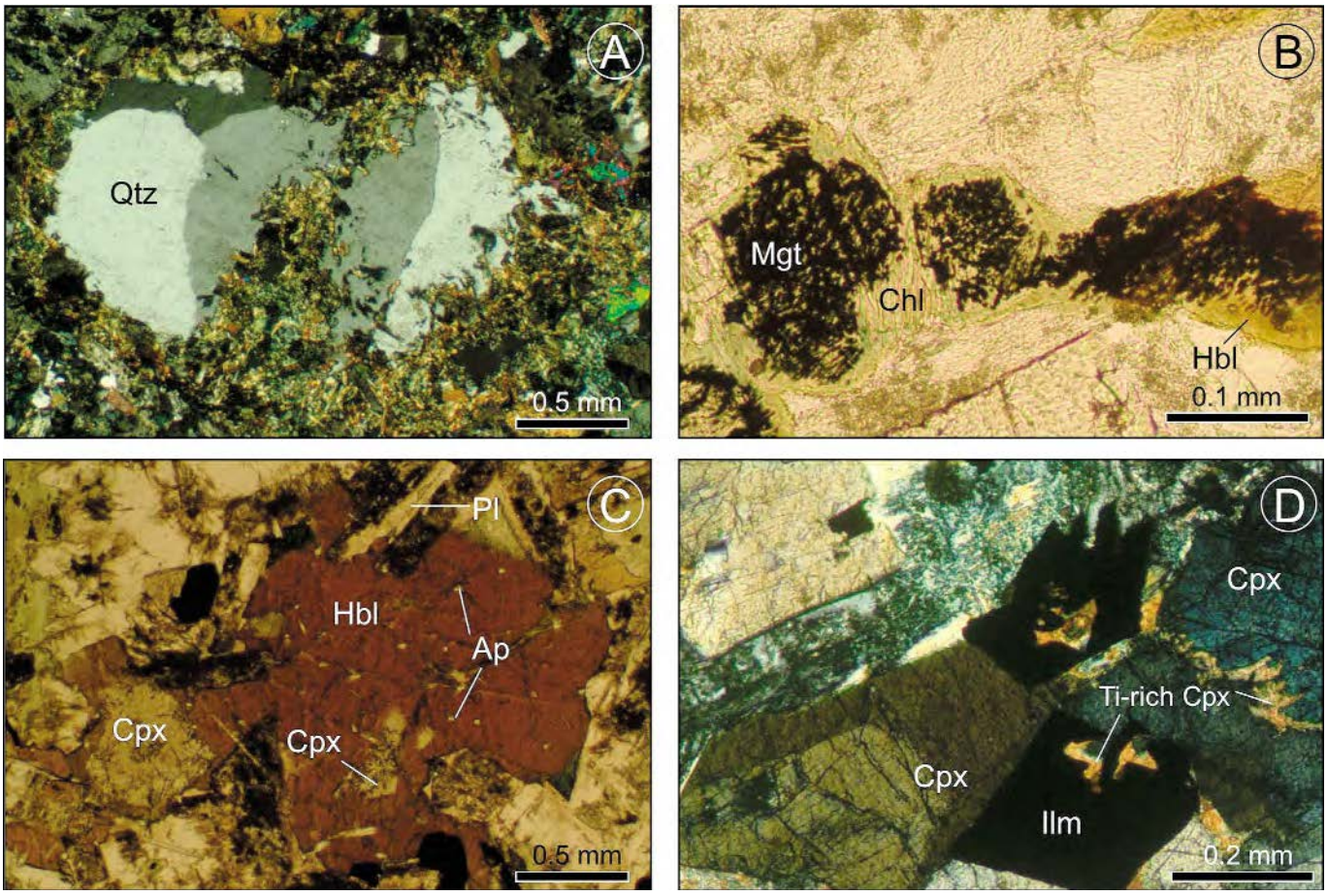

Fig. 2 - Representative transmitted light microphotographs of dolerite textures and compositions. Bar scale in photos. A- Crossed polars. Partially assimilated granitic xenocrysts in the Conca Verde dike. B- Plane polarized light. Chlorite + magnetite epita0ctic pseudomorphs on dehydrated hornblende phenocrysts. C- Plane polarized light. Hornblende overgrowths on clinopyroxene phenocryst poikilitic on needle-shaped to whisker apatite. D- Plane polarized light. Concentric zoned titanian-augite phenocrysts partially intergrown with skeletal ilmenites; intergrowth boundary zones and pyroxene cleavages are markedly Ti-enriched.

Table 2 - Representative analyses of clinopyroxenes.

Sample	LG32	LG32	LG108	LG108	LG38	LG87	LG87	LG19	LG19	LG51
Analysis	P3A1	P3A2	P1A1	P1A2	P1A1	P2A1	P2A2	P1A1	P1A6	P2A4
Occurrence	core	rim	core	rim	subhedral	poikilitic core	rim	groundmass	skeletal in groundmass	euhedral phenocryst
Classification	augite	augite	augite	augite	augite	augite	augite	titanian-augite	augite	augite
Symbol	Δ	Δ	Δ	Δ	□	□	□	■	■	●
Oxides wt%										
SiO_2	46.22	48.98	47.14	49.90	47.54	50.80	47.02	45.11	49.68	48.38
TiO_2	2.86	2.35	2.60	1.30	2.45	1.24	2.28	3.75	1.22	1.58
Cr_2O_3	0.46	0.27	0.24	0.18	0.30	0.27	0.31	0.32	0.32	0.28
Al_2O_3	5.25	3.21	5.81	2.96	4.81	1.88	4.50	5.83	1.58	3.51
FeO	10.09	11.29	9.34	11.07	10.03	9.24	9.57	11.21	12.02	10.26
MnO	0.35	0.52	0.23	0.36	0.35	0.42	0.31	0.42	0.48	0.37
MgO	12.12	11.51	11.56	11.60	13.08	14.71	12.91	11.07	13.91	14.53
NiO	0.29	0.24	0.16	0.07	0.23	0.22	0.19	0.24	0.25	0.18
CaO	21.99	21.75	21.68	21.79	21.35	20.96	21.45	21.44	19.68	19.85
Na_2O	0.00	0.17	0.00	0.00	0.03	0.58	0.27	0.16	0.24	0.64
K_2O	0.18	0.22	0.18	0.18	0.20	0.16	0.18	0.19	0.13	0.14
Total	100.18	100.63	98.94	99.41	100.70	100.95	99.43	100.08	99.93	100.42
Cations										
Si	1.748	1.850	1.797	1.901	1.780	1.879	1.780	1.719	1.878	1.803
Al^{IV}	0.234	0.143	0.203	0.099	0.212	0.082	0.201	0.262	0.070	0.154
Al^{VI}	0.000	0.000	0.058	0.034	0.000	0.000	0.000	0.000	0.000	0.000
Ti	0.081	0.067	0.075	0.037	0.069	0.035	0.065	0.107	0.035	0.044
Cr	0.014	0.008	0.007	0.005	0.009	0.008	0.009	0.010	0.010	0.008
Fe^{3+}	0.102	0.038	0.000	0.000	0.093	0.132	0.129	0.098	0.119	0.195
Fe^{2+}	0.218	0.319	0.298	0.353	0.221	0.154	0.174	0.259	0.261	0.125
Mn	0.011	0.017	0.007	0.012	0.011	0.013	0.010	0.014	0.015	0.012
Mg	0.683	0.648	0.657	0.659	0.730	0.811	0.728	0.629	0.784	0.807
Ni	0.009	0.007	0.005	0.002	0.007	0.007	0.006	0.007	0.008	0.005
Ca	0.891	0.880	0.885	0.889	0.856	0.831	0.870	0.875	0.797	0.793
Na	0.000	0.013	0.000	0.000	0.002	0.042	0.020	0.012	0.018	0.046
K	0.009	0.011	0.009	0.009	0.010	0.008	0.009	0.009	0.006	0.007
End-members										
Wollastonite	0.369	0.402	0.378	0.414	0.357	0.392	0.367	0.360	0.381	0.341
Enstatite	0.346	0.328	0.331	0.330	0.368	0.409	0.367	0.318	0.396	0.406
Ferrosilite	0.109	0.159	0.149	0.176	0.111	0.077	0.087	0.130	0.131	0.062

Table 3 - Representative analyses of amphiboles.

Sample	LG32	LG108	LG108	LG108	LG108	LG87	LG87	LG51	LG51	LG51	CPT1	CPT1	CPTC	CPTC
Analysis	P1A6	P2A5	P2A8	P3A2	P4A1	P1A3	P2A3	P1A1	P1A4	P2A6	P2A3	P2A4	P1A1	P1A3
Occurrence	Cpx overgrowth	groundmass	Cpx overgrowth	subhedral	subhedral	subhedral	Cpx overgrowth	subhedral in groundmass	groundmass	euhedral	micro-phenocryst core	micro-phenocryst rim	phenocryst core	phenocryst rim
Classification	pargasite	Fe-kaersutite	Fe-edenite	hastingsite	Mg-hastingsite	Mg-hastingsite	Mg-hornblende	Mg-homblende	Mg-hastingsite	Mg-hastingsite	Fe-kaersutite	kaersutite	pargasite	kaersutite
Symbol	Δ	Δ	Δ	Δ	Δ	□	□	●	●	●	▲	▲	▲	▲
Oxides wt%														
SiO_2	42.21	36.47	42.68	42.05	42.64	42.03	48.70	42.35	42.26	42.40	39.09	38.78	39.77	39.75
TiO_2	4.37	4.29	2.99	2.78	2.91	2.96	1.76	3.43	3.32	3.57	4.44	5.86	3.79	4.81
Cr_2O_3	0.13	0.05	0.02	0.00	0.14	0.22	0.20	0.21	0.21	0.19	0.15	0.06	0.12	0.14
Al_2O_3	8.87	12.45	8.63	9.58	9.84	9.59	3.38	9.79	9.53	9.64	13.46	12.83	14.04	13.17
FeO	15.50	26.12	19.74	19.93	18.61	15.45	19.75	14.97	18.08	16.10	17.36	11.15	15.92	12.23
MnO	0.33	0.56	0.30	0.29	0.45	0.52	0.68	0.48	0.38	0.39	0.20	0.16	0.20	0.23
MgO	10.82	2.33	8.76	8.80	9.90	11.27	11.38	12.12	9.67	11.34	8.44	12.45	9.49	11.36
NiO	0.16	0.00	0.00	0.00	0.02	0.35	0.20	0.10	0.10	0.07	0.00	0.00	0.00	0.04
CaO	11.07	9.74	10.48	10.62	10.27	10.80	9.38	11.01	11.24	11.16	9.85	11.60	10.34	11.96
Na_2O	3.73	3.18	3.36	3.58	3.66	3.91	2.24	1.88	2.65	2.07	3.30	3.66	2.22	2.53
K_2O	0.73	1.60	0.78	0.69	0.78	0.87	0.53	0.83	0.92	1.11	1.72	1.45	1.93	1.37
Total	97.92	96.79	97.74	98.32	99.22	97.97	98.20	97.17	98.36	98.04	98.01	98.00	97.82	97.59
Cations														
Si	6.414	5.912	6.532	6.396	6.353	6.340	7.163	6.277	6.381	6.310	5.931	5.837	5.950	5.982
Al^{IV}	1.586	2.088	1.468	1.604	1.647	1.660	0.586	1.710	1.619	1.690	2.069	2.163	2.050	2.018
Ti	0.499	0.523	0.344	0.318	0.326	0.336	0.195	0.382	0.377	0.400	0.507	0.663	0.427	0.544
Al^{VI}	0.002	0.290	0.089	0.114	0.081	0.045	0.000	0.000	0.077	0.001	0.338	0.112	0.426	0.317
Fe^{3+}	0.000	0.029	0.091	0.182	0.373	0.102	0.900	0.683	0.155	0.453	0.175	0.000	0.389	0.000
Cr	0.016	0.006	0.002	0.000	0.016	0.026	0.023	0.025	0.025	0.022	0.018	0.007	0.014	0.017
Mg	2.451	0.563	1.999	1.996	2.199	2.534	2.495	2.678	2.177	2.516	1.909	2.793	2.117	2.548
Fe^{2+}	1.970	3.511	2.436	2.353	1.946	1.847	1.529	1.173	2.128	1.551	2.203	1.403	1.603	1.539
Mn	0.042	0.077	0.039	0.037	0.057	0.066	0.085	0.060	0.049	0.049	0.026	0.020	0.025	0.029
Ni	0.020	0.000	0.000	0.000	0.002	0.042	0.024	0.012	0.012	0.008	0.000	0.000	0.000	0.005
Ca	1.791	1.693	1.722	1.738	1.654	1.750	1.510	1.777	1.825	1.799	1.608	1.856	1.673	1.917
$Na_{(B)}$	0.209	0.307	0.278	0.262	0.346	0.250	0.433	0.223	0.175	0.201	0.392	0.144	0.327	0.083
$Na_{(A)}$	0.884	0.693	0.722	0.799	0.721	0.896	0.219	0.327	0.604	0.403	0.583	0.915	0.323	0.651
K	0.141	0.331	0.153	0.134	0.150	0.168	0.102	0.160	0.178	0.213	0.334	0.276	0.372	0.262

more anorthitic plagioclase is affected by sericitization 3) titanite replaces ilmenite, 4) hornblende is replaced by actinolitic amphibole, 5) glass and/or interstitial mafic phases are replaced by chlorite.

Lamprophyre

The lamprophyre dike (Mt. Nieddu, south of Siniscola) has porphyritic texture (P.I. ≈ 15). The prevailing pargasite phenocrysts (up to 7 mm) are frequently poikilitic on apatite and ilmenite and show concentric zoning (Table 3). Needle-shaped apatite, zoned biotite and ilmenite phenocrysts are widespread. A panidiomorphic texture is well developed in the fine-grained groundmass that consists of plagioclase, amphibole, biotite, and Fe-oxide.

The host intrusives

The intrusive host complex is formed by granodiorites and diorites. Granodiorites have euhedral to subhedral biotite and rare allanite occur in poikilitic, zoned plagioclase megacrysts. Hornblende is an interstitial phase and frequently overgrows biotite; zoned plagioclase develops in medium- to fine-grained groundmass. Apatite, titanite, epidote, allanite are common accessory phases. Locally, widely-assimilated quartz and plagioclase xenoliths occur in fine-grained groundmass and green hornblende is a late-crystallized phase, frequently replacing biotite. Saussuritic alteration affects the plagioclase core and pistacite very occasionally rims allanite. The igneous assemblage of diorites is represented by markedly-zoned plagioclase with an anortitic core and lobated alkalic rims, euhedral biotite, poikilitic hornblende on biotite, quartz, sometimes poikilitic on plagioclase, poikilitic to interstitial titanite, interstitial epidote and needle-shaped apatite, generally included in other phases.

The Stazzo Sitagliaccio and Stazzo Piredda (granodiorites) and Coddu Vecchio (diorite) bodies provided the samples dated by $^{40}Ar/^{39}Ar$ method.

ANALYTICAL METHODS

Whole-rock major and trace element abundances for basalts were carried out with XRF techniques at the X-RAL Laboratories, Canada. Losses on ignition (LOI) were determined with the gravimetric method. RE elements were analyzed with ICP-MS at the X-RAL Laboratories, Canada.

The mineral phases were analysed at the University of Genoa using a Philips SEM 515 scanning electron microscope, equipped with an EDAX PV9100 spectrometer in the energy dispersive mode. Operating conditions were 15 kV accelerating voltage and 2.1 nA of beam current. Reference standards for the elements (in brackets) were: jadeite (Na), forsterite (Mg), albite (Al), augite (Si, Ca), microcline (K), ilmenite (Ti), chromite (Cr), rhodonite (Mn) and fayalite (Fe). Other elements were below detection limits. The natural standards were analysed by a WDS microprobe at Modena University. Na_2O and MgO contents analyzed in silicates by an EDS microprobe are generally underestimated if the analysis is processed with current automatic methods. To overcome this problem, the background for Na (1.040 keV) and Mg (1.252 keV) was manually corrected and considered to be between 0.9 and 4.2 keV. The manual background was corrected also for the natural standards. Raw data were reduced using the ZAF algorithm and the standard software of the EDAX PV9100.

The clinopyroxene analyses were calculated according to the stoichiometric method of simultaneous normalization to 4.00 cations and 6.00 oxygens, and Fe^{3+} = 12-total cation charge was considered for clinopyroxene. The allocation of cations to sites T, M_1 and M_2 was performed according to Morimoto et al. (1988). End members were calculated in the sequence: wollastonite, enstatite, ferrosilite, aegirine, jadeite, $CaAl_2SiO_6$, $CaFeAlSiO_6$, $CaCrAlSiO_6$, $CaTiAl_2O_6$. Morimoto et al. (1988) and the Rock (1990) nomenclature was adopted.

The Ca-amphibole cation sum was normalized to 13-(Ca + Na + K), as suggested by Leake et al. (1997); Fe^{3+} = 46-total cation charge and $Fe^{2+} = Fe_{tot}-Fe^{3+}$; Al^{VI} = 8-Si, $Al^{IV} = Al_{tot}-Al^{VI}$. The Leake et al. (1997) nomenclature was adopted. The plagioclase analyses were recalculated to total cations = 5 on the basis of eight oxygens. Ilmenites were recast on the basis of three oxygens.

The $^{40}Ar/^{39}Ar$ age determinations were carried out on amphibole phenocrysts separate from the Conca Verde dikes (samples LG51 and LG52). The separated fractions were analyzed with the $^{40}Ar/^{39}Ar$ incremental method at Actlab Laboratories (Canada). The samples wrapped in Al foil were loaded in evacuated and sealed quartz vials/an evacuated and sealed quartz vial with K and Ca salts and packets of LP-6 biotite interspersed with the samples to be used as a flux monitor. LP-6 biotite has an assumed age of 128.1 Ma. The samples were irradiated in a nuclear reactor for 48 hours. The neutron gradient did not exceed 0.5% of the sample size. The Ar isotope composition was measured with a Micromass 5400 static mass spectrometer. The 1200ºC blank of ^{40}Ar did not exceed $n*10^{-10}$ STP.

The Sr and Nd were analyzed at the Geochemistry Laboratory of Trieste University. Samples were dissolved in Teflon vials for isotopic analysis using a mixture of HF-HNO_3 and HCl-purified/purified HF-HNO_3 and HCl reagents. Sr and Nd were collected after ion exchange and reversed-phase chromatography, respectively; the total blank for Sr was less that 20 pg. The Sr and Nd isotopic compositions were obtained using a VG 54E mass spectrometer and "Analyst" software (Ludwig, 1994) for data acquisition and reduction. The $^{87}Sr/^{86}Sr$ and $^{143}Nd/^{144}Nd$ ratios were fractionation corrected to $^{86}Sr/^{88}Sr$ = 0.1194 and $^{146}Nd/^{144}Nd$ = 0.7219, respectively, and the measured ratios were corrected for instrumental bias to NBS 987 and La Jolla standard values of 0.71025 and 0.511860. The reported errors represent statistics at a 95% confidence level.

Nd-model ages were calculated with respect to a depleted mantle evolution curve given by eNd(T) = 0.25T^2-3T + 8.5 (T in Ga) as reported in Ludwig (1994).

MINERAL CHEMISTRY

Pyroxenes

Clinopyroxene ranges from diopside to augite (Wo_{34-41} $En_{31-42}Fs_{3-18}$), with high to remarkable titanium content (1.22-4.10 TiO_2 wt%).

Phenocrysts are weakly to strongly zoned with a Ti-rich core; in some dikes (e.g. at Stazzo Sitagliaccio) clinopyroxenes show normal Ti-rich and reverse zoning. The aegirine content is generally low (0-7 mole%), except at Conca Verde, with Ae-enriched cores.

In the groundmass, the clinopyroxenes have augite to titanian augite compositions (Table 2).

Table 4 - Representative analyses of feldspars.

Sample	LG32	LG32	LG32	LG38	LG38	LG87	LG87	LG87	LG19	LG19	CPT	CPT	CPT
Analysis	P2A4	P3A3	P1A4	P3A3	P3A2	P2A6	P2A7	P4A3	P1A3	P1A4	P3A1	P3A2	P3A4
Occurrence	euhedral	anhedral	interstitial	intergrowth Pl-Kfs	intergrowth Pl-Kfs	inclusion in poikilitic Cpx	inclusion in poikilitic Cpx	inclusion in high albite phenocryst	inclusion in high albite phenocryst	inclusion in oligoclase phenocryst	phenocryst core	phenocryst intermediate	phenocryst rim
Classification	labradorite	labradorite	andesine	high albite	K-feldspar	orthoclase	oligoclase	labradorite	andesine	orthoclase	oligoclase	sanidine	sanidine
Symbol	Δ	Δ	Δ	□	□	□	□	□	■	■	▲	▲	▲
Oxide wt%													
SiO_2	53.07	55.02	59.72	67.71	63.37	62.97	66.54	54.74	57.10	56.99	60.95	65.27	64.89
TiO_2	0.22	0.33	0.24	0.17	0.43	0.41	0.20	0.16	0.27	0.22	0.22	0.09	0.10
Al_2O_3	28.63	27.46	24.91	20.41	18.06	17.83	20.87	28.37	26.07	25.04	23.35	18.78	18.32
Cr_2O_3	0.15	0.20	0.11	0.14	0.14	0.11	0.15	0.08	0.21	0.13	0.06	0.06	0.03
FeO	0.99	0.80	0.44	0.20	0.00	0.00	0.32	0.43	0.87	0.00	0.24	0.00	0.26
Fe_2O_3	0.00	0.00	0.00	0.00	0.20	0.34	0.00	0.19	0.00	1.74	0.00	0.33	0.00
MgO	0.00	0.00	0.00	0.00	0.00	0.44	0.00	0.00	0.00	0.00	0.00	0.08	0.00
MnO	0.10	0.13	0.02	0.16	0.09	0.07	0.16	0.00	0.07	0.03	0.00	0.06	0.09
CaO	12.91	11.24	7.56	1.55	0.22	0.28	2.05	10.46	9.01	0.28	5.57	1.36	0.98
Na_2O	3.73	4.57	6.73	9.94	0.00	0.33	9.69	5.23	5.78	0.79	7.38	6.11	3.87
K_2O	0.25	0.26	0.43	0.27	17.16	16.72	0.29	0.34	0.58	14.14	1.51	7.58	9.24
NiO	0.12	0.22	0.08	0.01	0.08	0.07	0.13	0.00	0.13	0.10	0.00	0.06	0.00
Totale	100.19	100.25	100.25	100.53	99.74	99.56	100.40	100.00	100.10	99.46	99.28	99.78	97.78
Cations													
Si	2.423	2.501	2.678	2.981	2.948	2.924	2.937	2.474	2.579	2.637	2.743	2.941	3.026
Ti	0.008	0.011	0.008	0.006	0.015	0.014	0.007	0.006	0.009	0.008	0.007	0.003	0.004
Cr	0.006	0.007	0.004	0.005	0.005	0.004	0.005	0.003	0.008	0.005	0.002	0.002	0.001
Al	1.541	1.471	1.317	1.059	0.990	0.976	1.086	1.511	1.388	1.365	1.238	0.997	1.006
Fe^{3+}	0.000	0.000	0.000	0.000	0.007	0.012	0.000	0.007	0.000	0.061	0.000	0.011	0.000
Fe^{2+}	0.038	0.030	0.017	0.007	0.000	0.000	0.012	0.016	0.033	0.000	0.009	0.000	0.010
Mn	0.004	0.005	0.001	0.006	0.004	0.003	0.006	0.000	0.003	0.001	0.000	0.002	0.004
Mg	0.000	0.000	0.000	0.000	0.000	0.031	0.000	0.000	0.000	0.000	0.000	0.005	0.000
Ni	0.005	0.008	0.003	0.000	0.003	0.003	0.005	0.000	0.005	0.004	0.000	0.002	0.000
Ca	0.632	0.548	0.363	0.073	0.011	0.014	0.097	0.506	0.436	0.014	0.269	0.066	0.049
Na	0.330	0.403	0.585	0.848	0.000	0.029	0.829	0.459	0.506	0.071	0.644	0.534	0.350
K	0.015	0.015	0.025	0.015	1.018	0.991	0.016	0.020	0.033	0.835	0.087	0.436	0.550
End-members													
Albite	0.338	0.417	0.601	0.906	0.000	0.028	0.880	0.466	0.519	0.077	0.644	0.516	0.369
Anorthite	0.647	0.567	0.373	0.078	0.011	0.013	0.103	0.514	0.447	0.015	0.269	0.063	0.052
Orthoclase	0.015	0.016	0.025	0.016	0.989	0.958	0.017	0.020	0.034	0.908	0.087	0.421	0.579

Amphiboles

Igneous amphiboles have calcic compositions (magnesio-hastingsite, hastingsite, ferro-edenite, ferro-pargasite, ferro-kaersutite, tschermakite and magnesio-hornblende after Leake et al., 1997 classification), and are characterized by low SiO_2 (36.47 wt% in ferro-kaersutite to 42.68 wt% in ferro-edenite) and Al_2O_3 in the range 8.63-12.45 wt%. The Al-Si substitution in the tetrahedric site (Al = 1.5-2 a.p.f.u.) matches the potassium increase in the A site (K up to 0.33 a.p.f.u.). The $Mg/(Mg + Fe^{2+})$ ratio of interstitial amphiboles is in the range 0.14-0.58, suggesting their precipitation from a Fe-enriched residual liquid.

In the Mt. Nieddu lamprophyre, amphiboles are calcic and have predominant kaersutitic and pargasitic with subordinate ferro-pargasitic compositions; rare ferro-kaersutitic and magnesio-hastingsite compositions also occur (Leake et al., 1997). The relevant Ti content ranges between 0.40 and 0.71 a.p.f.u. (Fig. 3A). Commonly, zoned phenocrysts show a core-to-rim increase of Ti and Mg#, evolving from ferro-pargasite/pargasite to pargasite/kaersutite. The microphenocrysts show pargasite/ferro-kaersutite to kaersutite core-to-rim zoning. In amphibole phenocrysts, Baldelli et al. (1987) found a reverse zoning with a ferroan-pargasitic core and a kaersutitic rim. Some amphiboles are characterized by significant pargasitic-barroisitic substitution (Fig. 3B), the Na content in site B reaching up to 0.43 a.p.f.u..

Feldspars

K-feldspar phenocrysts are often albitized ($Ab_{90-97}An_{2-8}Or_{1-2}$); feldspar inclusions in clinopyroxene phenocrysts have an oligoclase to labradorite (An_{51}) composition, with a minor orthoclase solid solution (~2-3 mole%), or K-feldspar composition. Groundmass interstitial plagioclase has an albite composition (An_{5-8}), and occurs in association with exsolved or intergrown K-feldspar. In K-feldspar-free dikes, plagioclase phenocrysts have a labradorite composition (An_{57-65}), with a minor orthoclase solid solution (~ 1.5 mole%); interstitial plagioclase has an oligoclase to andesine composition (An_{15-37}) with orthoclase in the range 2-4 mole%. Representative feldspar compositions are in Table 4.

At Mt. Nieddu, feldspar microcrysts (up to 0.26 mm) in groundmass aggregates show clear compositional zoning with an oligoclase core (An_{27}) and high-K rim (Or_{37}). Interstitial feldspars are pure albite or sodic K-feldspar with An up to 3 mole% ($Or_{78}An_{29}$). In the potassic rim of feldspar microcrysts, An reaches up to 6 mole%. Both perthite and antiperthite exsolutions were found.

Biotites

The brown micas of the lamprophyric dike have been classified as biotites (Fig. 4) on the basis of the Fe/(Mg + Fe) vs. silica diagram (Rieder et al., 1998). Phenocrysts intergrown with ilmenite/Ti-magnetite, titanite and amphibole, have a homogeneous composition with a predominant eastonite molecule (Al^{IV} = 2.70 a.p.f.u.), subordinate annite (Fe^{2+} = 0.88 - 0.94 a.p.f.u.) and very high titanium content (Ti in the range 0.79 - 0.82 a.p.f.u.). Late-magmatic biotites, cotectic with oxides (Usp_{67-68} Mgt_{19-22}), show a more important annite end-member (Fe^{2+} = 2.55 - 3.06 a.p.f.u.) and considerable titanium content (Ti in the range 0.41 - 0.69 a.p.f.u.); the siderophyllite molecule occurs rarely (Al^{VI} = 0.44 a.p.f.u). All the biotite phenocrysts contain Fe^{3+} up to 1.24 a.p.f.u.

Oxides

Subhedral to skeletal ilmenite includes a significant pyrophanite ($MnTiO_3$) component (up to 6.8 MnO wt%). Its composition varies between $Ilm_{88}Hem_5Pyr_7$ and $Ilm_{81}Hem_4Pyr_{15}$.

The oxide phenocrysts of the lamprophyre have Usp_{67-68} Mgt_{19-22} compositions evolving toward the ulvospinel end-member from core to rim.

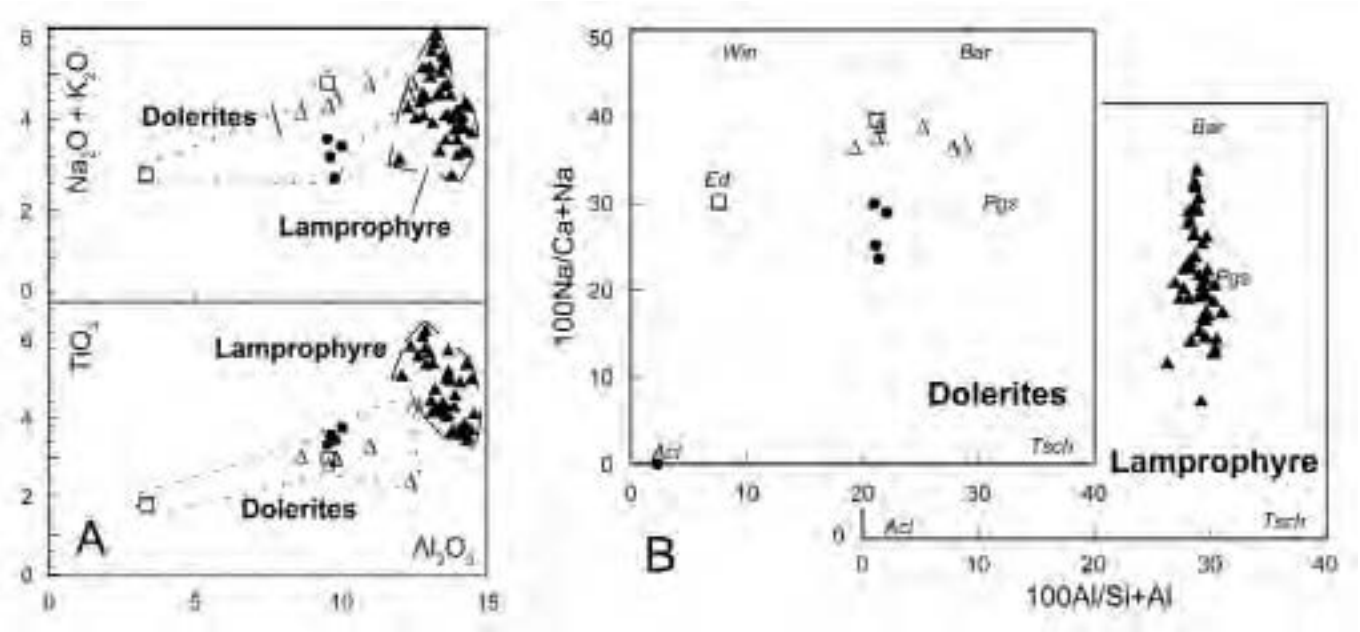

Fig. 3 - A) $Na_2O + K_2O$ vs. Al_2O_3 and TiO_2 vs. Al_2O_3 for amphiboles. B) 100 (Na/Ca + Na) vs. 100 (Al/Al + Si) diagrams (Laird and Albee, 1981) for amphiboles. Plotted amphibole compositions are distinguished by different lithologies: sub-alkalic basalts: empty triangle; transitional basalts: empty square; K-trachybasalts and mugearites from Conca Verde: filled circle; tephritic lamprophyre: filled triangle.

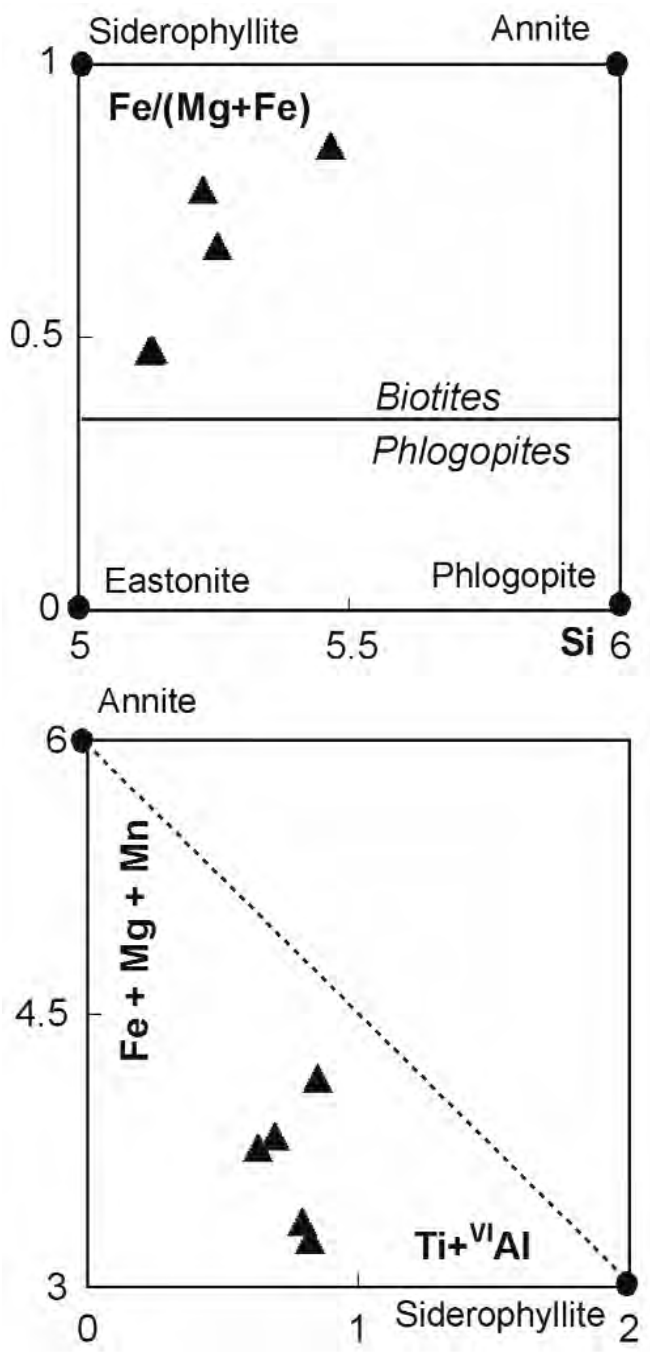

Fig. 4 - Classification diagram for brown micas of the Mt. Nieddu lamprophyre dike (Rieder et al., 1998).

GEOCHEMICAL CHARACTERISTICS

The dolerites range in composition from sub-alkalic to alkalic basalts, with prevalent transitional basalts (TAS diagram, not reported); hawaiites, K-trachybasalts, mugearites and shoshonites represent subordinate compositions.

Dolerites show a large compositional range with SiO_2 between 43.56 and 51.69 wt%. In the Nb/Y-TiO_2/Zr diagram (Winchester and Floyd, 1977; Fig. 5) the samples fall in the andesite to sub-alkalic basalt fields. Relatively evolved compositions correspond to Mg# in the range 50-29. TiO_2, Na_2O, P_2O_5, and Y are inversely correlated with Mg#; positive correlations are highlighted for CaO, Ni, Cr, Nb and in part Al_2O_3 (Fig. 6).

Positive correlations of Al and Ca with Mg# suggest fractionation of Ca-rich plagioclase and, to a minor extent, augite, whereas a positive Ni and Cr correlation with Mg# describes olivine and spinel fractionation respectively, followed by clinopyroxene. The negative correlations of Ti and Na with Mg# indicate their enrichment in the residual liquid in accordance with the crystallization of interstitial ilmenite and the precipitation of albitic plagioclase with consequent significant plagioclase zoning. Y and P negative correlations are consistent with the late precipitation of apatite and/or hornblende (Y). Higher concentrations of phenocrysts, also increasing in grain size, towards the center of the St. Pantaleo dike (e.g. + 8% modal olivine, + 7% modal clinopyroxene) are interpreted as due to grain dispersive pressures (Bagnold effect) during laminar flow causing a flow differentiation process (Komar, 1972). The increasing Ni and Cr toward the center of the St. Pantaleo dike matches the petrographic evidence; the Si enrichment toward the margins can be related to an increase in the fine-grained groundmass or, more probably, to wall-rock assimilation.

Significant major and trace element variations occur between margin and core of the St. Pantaleo dike, where Ni, Cr and incompatible trace element contents (Zr, Y, Sr) increase and SiO_2 decreases. The margin is also characterized by lower ΣREE content (46.75 ppm) than the core (74.09 ppm) (Fig. 7A).

The normalized REE-chondrite patterns (Fig. 7) are relatively homogeneous and show poor (La_N/Yb_N = 1.48) to slightly fractionated patterns (La_N/Yb_N = 4.43). Relatively primitive dolerites show REE patterns about 20 times that of chondrite (St. Pantaleo); the Li Reni dolerite LREE reaches 50 times that of chondrite and has a negative Sm anomaly. The Mt. E'Senes dike has flat LREE and HREE patterns (respectively 40 and 20 times that of chondrite; La_N/Yb_N = 3), slightly fractionated MREE and a weak negative Eu anomaly.

The MORB-normalized spiderdiagrams (Fig. 8) show LFSE enrichment (Table 5A-B) in particular for Rb and Ba, markedly increasing from primitive to evolved terms (e.g. for Montiferru di Tertenia dolerites, Ba ranges between 117 and 161). HFSE abundances are vaguely comparable with OIB patterns (after Sun, 1980).

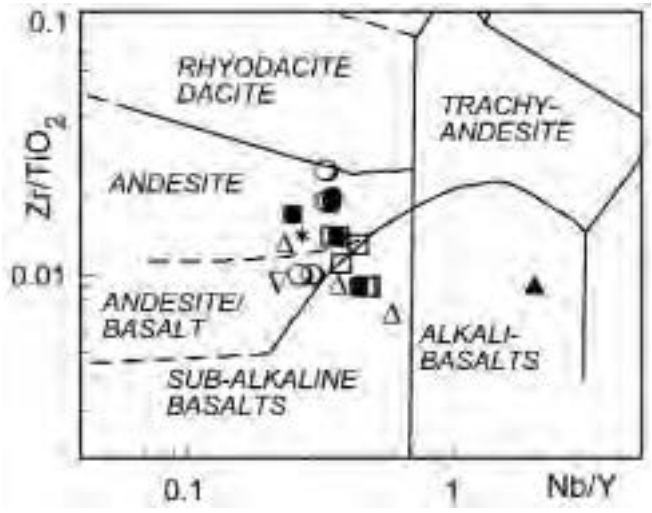

Fig. 5 - Zr/TiO_2 versus Nb/Y classification diagram (Winchester and Floyd, 1977). Symbols: sub-alkalic basalts: empty triangle; transitional basalts: empty squares; hawaiites: filled squares; K-trachybasalts and shoshonites: empty circles; mugearites: stars; sub-alkalic basalts from Li Reni: inverted empty triangles; K-trachybasalts and mugearites from Conca Verde: filled circles; tephritic lamprophyres: filled triangles.

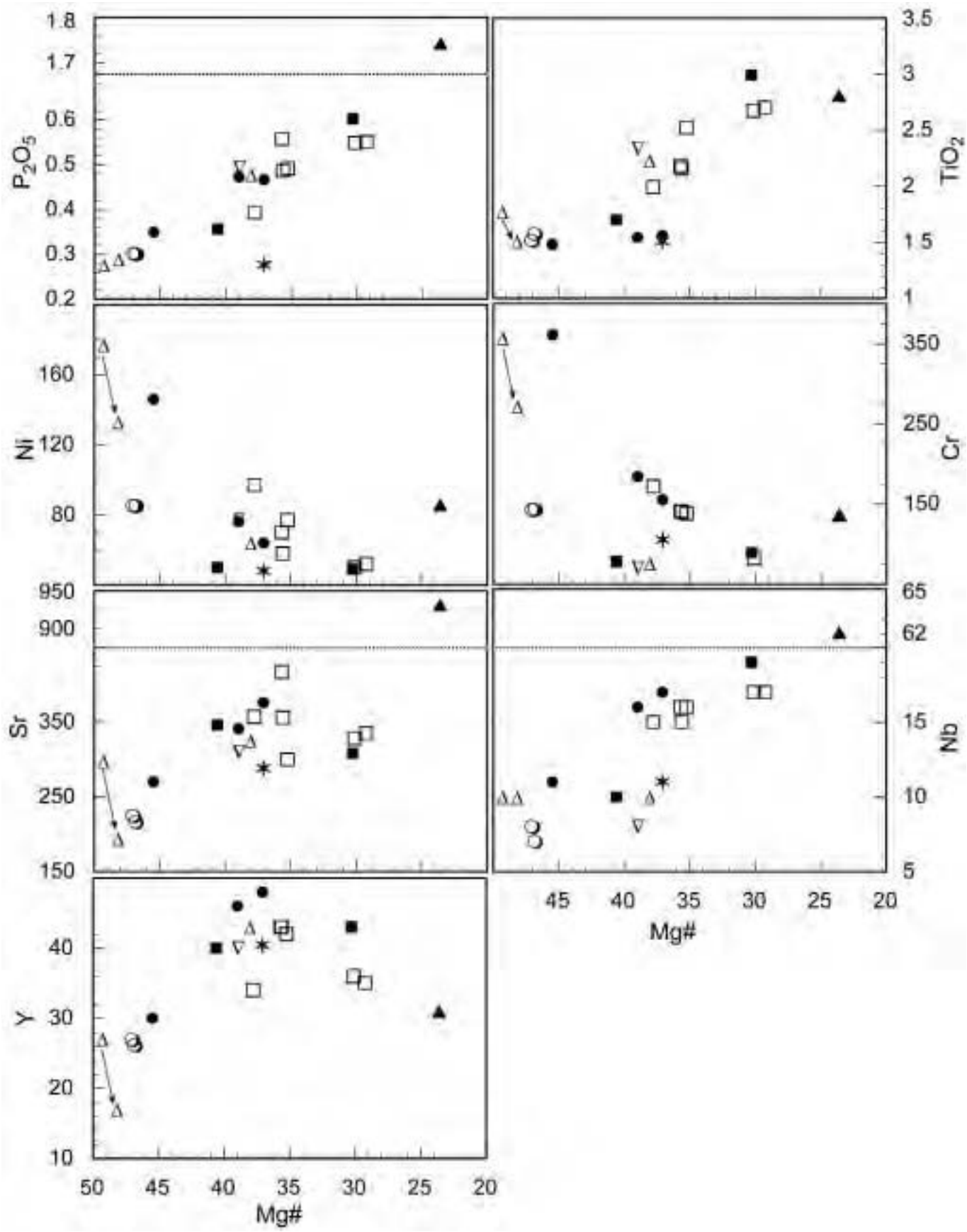

Fig. 6 - Selected major and trace elements Mg#-variation diagrams. Arrows indicate core-to-margin compositional variations in the St. Pantaleo dike.

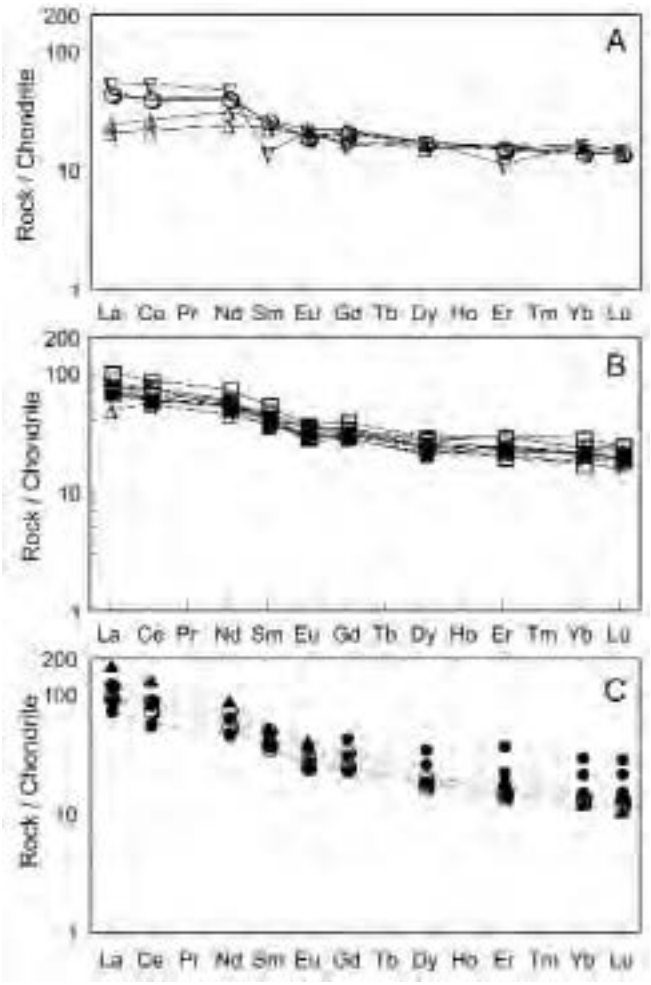

Fig. 7 - Chondrite-normalized REE patterns (Nakamura, 1974). Sub-alkalic basalts from St. Pantaleo, Li Reni and K-trachybasalt from Mt. E'Senes are plotted in Fig. 7A, transitional basalt and shoshonites from Montiferru di Tertenia, K-trachybasalt and mugearites from Conca Verde and tephritic lamprophyre from Mt. Nieddu are plotted in Fig. 7C, the others in Fig. 7B.

An intraplate tholeiitic affinity arises for dolerites in the 2Nb-Zr/4-Y diagram (Fig. 9A); the signature is confirmed on the basis of the La/10-Y/15-Nb/8 (Cabanis and Lecolle, 1989; Fig. 9B) where dolerites mostly fall in the continental basalt field, except for the St. Pantaleo dike, which is an E-MORB. A higher Zr content in dolerites could be the consequence of an inherited, Zrc-enriched crustal component. A further petrogenetic clue is obtained from the Tbx3-Th-Ta diagram (Fig. 9C), where dolerites, with transitional to tholeiitic basalt compositions, except for Conca Verde, Penisola Coluccia, Calangianus and Mt. E'Senes, indicate an anorogenic regime.

The Mt. Nieddu lamprophyre has a tephrite composition (normative olivine = 5.62) and alkali-basalt composition in the Nb/Y-TiO_2/Zr diagram (Winchester and Floyd, 1977). The lamprophyre has low Mg# and very high concentrations of P, K, Ba, Sr and Nb, consistent with the apatite and K-feldspar modal abundances (Fig. 6, Table 5B). The REE patterns are fractionated (La_N/Yb_N = 14.27) with high LREE.

The MORB-normalization for the Mt. Nieddu lamprophyre shows high LILE (Rb, Ba, K) abundances, comparable with the upper crust (Taylor and McLennan, 1981), and the lack of Nb and Sr negative anomaly that conversely characterizes dolerite patterns, with Nb and Sr enrichments comparable to OIBs (Sun, 1980). The petrographic evidence, the Nb/Y ratio and inter-elemental correlations consistently suggest a non-cogenetic relationship between dolerites and lamprophyre.

The tephrite lamprophyre, on the whole comparable with the alkalic dikes of Sardinia, Corsica (near Zonza, southern Corsica, Traversa et al., 2003) and Provence, is ascribed to anorogenic affinity.

To estimate the effects of concurrent assimilation and crystal fractionation from the most primitive magmas to the most evolved dolerite compositions, we used De Paolo's equation (1981) for trace element modeling. The average (over 16 samples) composition of the Arzachena monzogranite facies has been assumed as a contaminant. The wide range of abundances for some elements in the monzogranite (e.g. Ba between 207 and 1181 ppm) and the U spike in the chondrite-normalized spiderdiagrams (not reported) for the contaminated magma suggested to select one composition rather than using an average value. The best fit was obtained for sample AA39 at 0.4 *r* (ratio of the rate of assimilation to the rate of crystallization), corresponding to a fraction of remaining magma (F) between 70% and 80%, appropriate for Conca Verde dolerite compositions (Fig. 10).

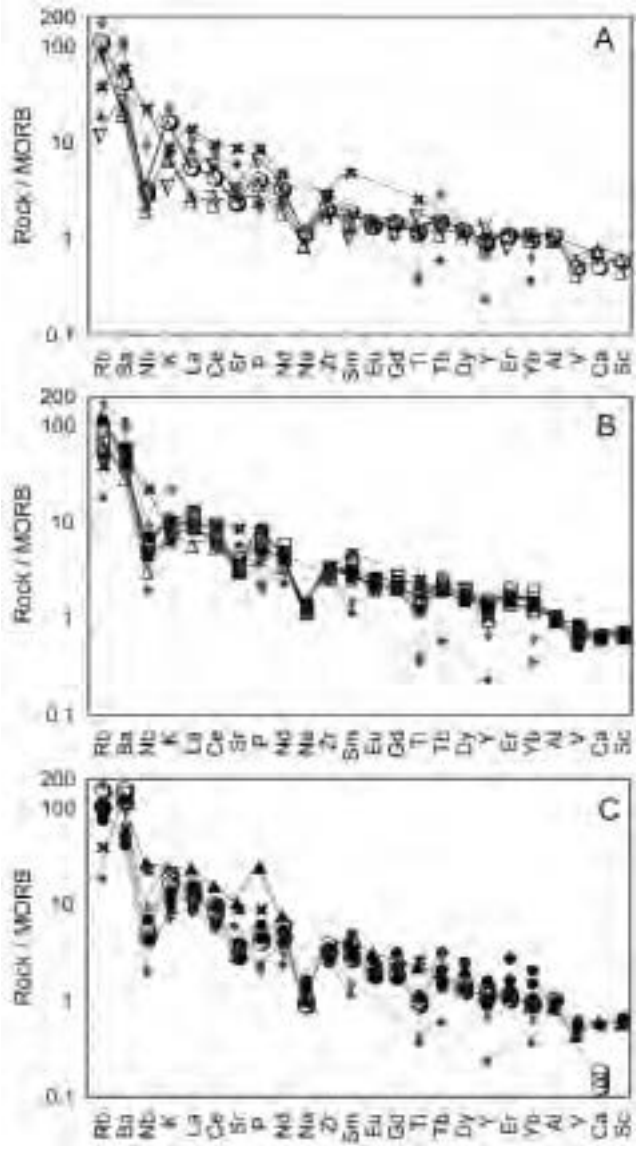

Fig. 8 - MORB-normalized spiderdiagram (Pearce and Parkinson, 1993). Upper crust: light grey diamond; lower crust: dark grey diamond; OIB: cross. Symbols as in Fig. 5.

Table 5a - Bulk rock compositions: major and trace element compositions for sub-alkalic and transitional basalts (a) and for hawaiites, K-trachybasalts, mugearites, shoshonites and tephritic lamprophyre (b); Rare Earth Element compositions in (c).

Sample	LG32	LG33	SG20	LG108	LG38	LG87	LG101	LG103	LG127	EB13
Lithology	sub-alkalic basalt	sub-alkalic basalt	sub-alkalic basalt	transitional basalt	transitional basalt	transitional basalt	transitional basalt	transitional basalt	transitional basalt	transitional basalt
Provenance	S. Pantaleo	S. Pantaleo	Li Reni	Palau	Mirialveda	Montigrossu	Costa Serena	Porto Rafael	Penisola Coluccia	Montiferru di Tertenia
Symbol	Δ	Δ	∇	Δ	□	□	□	□	□	❍
Oxide (wt%)										
SiO_2	47.91	43.56	46.40	44.27	45.03	45.14	44.49	44.63	47.54	48.08
TiO_2	1.52	1.67	2.28	2.11	2.55	1.87	2.03	2.36	2.04	1.24
Al_2O_3	16.94	15.84	16.50	16.05	15.68	16.03	16.44	15.15	15.03	16.04
Cr_2O_3	0.04	0.06	0.01	0.01	0.01	0.02	0.02	0.02	0.02	n.a.
$Fe_2O_{3\ t}$	10.60	10.16	12.20	11.22	12.41	10.80	11.04	12.06	10.71	9.10
MgO	9.85	9.87	7.96	6.89	5.30	6.75	6.31	6.76	6.10	13.47
MnO	0.18	0.18	0.14	0.20	0.18	0.17	0.19	0.20	0.18	0.15
CaO	9.55	9.14	8.23	8.74	7.92	8.19	7.57	7.23	7.81	1.79
Na_2O	2.48	2.61	2.94	3.46	3.78	3.45	3.23	3.43	3.36	2.47
K_2O	0.97	0.88	0.46	0.92	1.08	1.18	1.34	1.33	1.24	2.03
P_2O_5	0.29	0.26	0.48	0.45	0.52	0.37	0.52	0.46	0.46	0.33
LOI	3.60	4.10	2.45	3.00	2.90	2.80	4.50	3.70	3.10	5.30
Sum	104.00	98.39	100.10	97.43	97.45	96.90	97.82	97.45	97.71	100.00
Trace Elements (ppm)										
Ag	<1	<1	n.a.	<1	<1	<1	1	2	1	n.a.
Ba	78	135	179	198	228	364	403	347	313	740
Co	47.7	61.3	n.a.	82.3	59.8	66.6	54.7	52	54.9	42
Cr	273	435	70	72		145	147	146	145	200
Cs	1.7	1.9	n.a.	1.8	0.5	0.6	0.9	1.2	0.7	n.a.
Cu	57	55	n.a.	41	41	44	35	39	28	18
Ga	11	17	n.a.	21	23	21	20	21	19	20
Hf	2	3	n.a.	6	6	6	6	6	6	n.a.
Mo	<2	<2	n.a.	<2	<2	<2	<2	<2	<2	n.a.
Nb	<10	<10	8	<10	17	15	16	16	15	11
Ni	133	177	77	64	52	97	70	77	58	99
Pb	<5	<5	n.a.	<5	<5	<5	9	<5	<5	5
Rb	40.4	50.7	7	33.5	40.1	35.7	53.1	56.2	39.7	58
Sc	20	27	n.a.	30	25	27	27	29	29	38
Sn	2	2	n.a.	3	2	2	2	3	2	n.a.
Sr	194	298	310	325	335	357	417	300	356	350
Ta	<0.5	0.6	n.a.	1.4	2	1.6	1.5	1.5	1.7	n.a.
Th	0.3	0.2	0.9	1	2	2.1	2.1	1.9	4	5
Tl	<0.5	<0.5	n.a.	<0.5	<0.5	<0.5	<0.5	<0.5	<0.5	n.a.
U	0.09	0.08	0.1	0.26	0.56	0.52	0.94	0.49	0.78	3
V	139	195	n.a.	203	253	210	202	228	206	n.a.
W	138	156	n.a.	490	421	384	217	159	334	n.a.
Y	17	27	40	43	35	34	43	42	43	32
Zn	59	90	n.a.	100	117	93	107	123	106	175
Zr	102	152	214	290	238	264	295	285	297	245
Mg#	48.17	49.28	39.48	38.05	29.93	38.46	36.37	35.92	36.29	59.68
Th/Ta	0.60	0.33	-	0.71	1.00	1.31	1.40	1.27	2.35	-
La/Nb	0.46	0.71	2.13	1.69	1.16	1.53	1.67	1.37	1.85	2.75

Table 5b

Sample	LG19	LG60	FR 38	LG52	LG51	LG53	FE12	EB7A	EB16	CPT1
Lithology	hawaiite	hawaiite	potassic-trachybasalt	potassic-trachybasalt	mugearite	mugearite	mugearite	shoshonite	shoshonite	tephritic lamprophyre
Provenance	Cupalchiata	Stazzo Pietraniedda	M.E'Senes	Conca Verde	Conca Verde	Conca Verde	Calangianus	Montiferru di Tertenia	Montiferru di Tertenia	M.Nieddu
Symbol	■	■	❍	●	●	●	*	❍	❍	▲
Oxide (wt%)										
SiO_2	44.56	46.92	46.11	47.44	51.64	51.69	52.81	52.85	48.84	43.66
TiO_2	2.83	1.62	1.46	1.40	1.47	1.47	1.47	1.13	1.18	2.83
Al_2O_3	14.82	16.45	17.51	15.73	15.19	15.00	16.70	16.51	15.87	13.53
Cr_2O_3	<0.01	<0.01	0.02	0.05	0.02	0.02	0.02	n.a.	n.a.	0.02
$Fe_2O_{3\ t}$	13.35	9.76	10.29	9.34	8.47	7.94	8.79	8.29	8.98	19.52
MgO	5.80	6.67	9.13	7.79	5.41	4.68	5.18	10.07	11.85	6.03
MnO	0.21	0.17	0.26	0.16	0.15	0.13	0.15	0.15	0.15	0.23
CaO	7.50	8.34	6.14	6.80	6.63	6.68	6.89	1.51	2.16	7.35
Na_2O	3.69	4.20	3.12	3.62	4.22	4.57	3.85	2.41	2.78	2.83
K_2O	1.26	0.84	2.14	1.77	1.54	1.69	1.45	2.61	2.08	3.13
P_2O_5	0.57	0.34	0.29	0.33	0.45	0.44	0.27	0.33	0.28	1.76
LOI	3.40	2.40	3.90	3.10	2.60	2.00	2.49	4.14	5.82	3.00
Sum	98.12	97.83	100.40	97.63	97.92	96.44	100.20	100.00	99.99	104.20
Trace Elements (ppm)										
Ag	<1	1	<1	<1	1	1	1	n.a.	n.a.	1
Ba	294	249	277	330	285	268	361	930	1015	806
Co	57.2	69	51.1	52.8	51.4	57.6	59.1	56	40	102
Cr	72	72		362	144	145	105	265	175	135
Cs	1.3	0.5	0.9	0.9	0.7	0.4	1.4	n.a.	n.a.	1.2
Cu	45	34	32	35	26	23	38	13	16	46
Ga	23	21	17	18	21	21	21	21	18	19
Hf	6	6	4	4	6	7	6	n.a.	n.a.	6
Mo	<2	<2	<2	<2	<2	<2	<2	n.a.	n.a.	5
Nb	19	<10	8	11	16	17	11	13	11	62
Ni	49	50	85	146	76	64	48	77	78	85
Pb	5	6	<5	9	<5	<5	n.a.	45	6	8
Rb	66.8	28.5	65.4	58.5	45.6	42.8	70.8	89	60	65
Sc	31	26		28	26	24	27	31	35	23
Sn	2	3	1	2	2	3	2	n.a.	n.a.	2
Sr	308	346	224	270	341	376	288	275	265	930
Ta	1.9	1.4	0.7	1.2	1.7	2.3	1.3	n.a.	n.a.	5
Th	2.2	1.8	1.3	3.5	6.5	6.9	10.3	7	5	5.6
Tl	<0.5	<0.5	<0.5	<0.5	<0.5	<0.5	<0.5	n.a.	n.a.	<0.5
U	0.58	0.35	0.28	0.79	1.34	1.39	1.11	<2	5	1.97
V	278	165	156	191	159	166	209	n.a.	n.a.	131
W	249	494	57	148	378	602	194	n.a.	n.a.	381
Y	43	40	26.9	30	46	48	40.4	39	33	30.8
Zn	135	92	105	95	82	76	111	160	135	135
Zr	280	287	155	200	286	304	207	295	235	259
Mg#	30.29	40.60	47.01	45.48	38.98	37.08	37.08	54.85	56.89	23.60
Th/Ta	1.16	1.29	1.86	2.92	3.82	3.00	7.92	-	-	1.12
La/Nb	1.18	1.80	1.79	1.84	1.92	1.95	2.40	3.08	2.90	0.93

Table 5c

Sample	LG32	LG33	SG20	LG108	LG38	LG87	LG101	LG103	LG127	EB13	LG19	LG60	FR 38	LG52	LG51	LG53	FE12	EB7A	EB16	CPT1
Symbol	Δ	Δ	∇	Δ	□	□	□	□	□	❍	■	■	❍	●	●	●	*	❍	❍	▲
Rare Earth Elements (ppm)																				
La	4.60	7.10	17.00	16.90	19.80	22.90	26.70	21.90	27.80	30.30	22.40	18.00	14.30	20.20	30.70	33.10	26.40	40.10	31.90	57.60
Ce	12.90	20.50	45.30	45.20	46.20	55.10	62.70	52.50	63.60	65.50	53.20	45.60	33.90	45.80	68.80	76.20	64.00	77.80	63.20	116.00
Pr	2.12	3.49	5.50	6.99	6.76	7.75	8.91	7.61	8.97	n.a.	7.58	6.70	5.17	6.42	9.79	10.60	8.18	n.a.	n.a.	14.30
Nd	10.60	17.00	29.10	32.10	30.80	33.30	39.30	33.70	38.40	35.30	34.70	29.80	25.00	27.70	41.30	44.60	37.40	46.90	33.80	56.00
Sm	2.70	4.70	2.80	7.80	7.10	7.40	9.20	8.00	8.50	8.10	8.60	6.70	5.20	6.10	9.00	9.70	8.90	10.50	7.30	10.80
Eu	1.02	1.60	1.61	2.51	2.37	2.16	2.43	2.42	2.30	1.90	2.66	2.20	1.45	1.71	2.28	2.48	2.03	2.38	1.95	3.18
Gd	3.42	4.98	4.40	8.58	7.80	7.91	8.73	8.90	8.89	7.20	8.96	7.98	5.68	6.23	9.60	9.80	7.77	9.30	6.80	19.00
Tb	0.59	0.88	1.00	1.38	1.28	1.21	1.46	1.38	1.42	n.a.	1.41	1.25	1.04	0.97	1.51	1.56	1.30	n.a.	n.a.	1.31
Dy	3.34	5.35	5.80	8.54	7.44	7.14	8.15	8.15	7.97	6.20	8.01	7.42	5.78	5.92	8.49	9.05	7.32	7.00	5.80	6.44
Ho	0.73	1.14	1.00	1.76	1.46	1.49	1.63	1.67	1.65	n.a.	1.66	1.52	1.18	1.10	1.79	1.86	1.63	n.a.	n.a.	1.12
Er	2.20	3.25	2.50	5.15	4.11	3.98	4.94	4.86	4.68	3.30	4.73	4.54	3.27	3.36	5.14	5.50	4.65	3.60	3.10	3.30
Tm	0.31	0.45	0.50	0.66	0.57	0.60	0.66	0.61	0.64	n.a.	0.65	0.64	0.45	0.46	0.70	0.73	0.67	n.a.	n.a.	0.40
Yb	1.90	3.20	3.50	5.00	3.60	3.90	4.30	4.30	4.40	3.10	4.30	4.50	3.00	3.20	4.80	5.00	3.90	2.90	2.80	2.70
Lu	0.32	0.45	0.50	0.73	0.61	0.60	0.70	0.69	0.63	0.45	0.63	0.66	0.46	0.49	0.70	0.73	0.52	0.45	0.41	0.36
La/Sm	1.05	0.93	3.75	1.34	1.72	1.91	1.79	1.69	2.02	2.31	1.61	1.66	1.70	2.04	2.10	2.11	1.83	2.36	2.70	3.29
Gd/Yb	1.43	1.24	1.00	1.37	1.73	1.62	1.62	1.65	1.61	1.85	1.66	1.41	1.51	1.55	1.59	1.56	1.59	2.56	1.94	5.61
La/Yb	1.62	1.48	3.25	2.26	3.68	3.93	4.15	3.41	4.22	6.54	3.48	2.67	3.19	4.22	4.28	4.43	4.53	9.25	7.62	14.27
SREE	46.75	74.09	120.5	143.3	139.9	155.4	179.8	156.7	179.9	161.4	159.5	137.5	105.9	129.7	194.6	210.9	174.7	200.9	157.1	292.5
Eu/Eu*	0.95	1.25	1.86	2.03	1.92	1.70	1.70	1.98	1.77	1.24	2.04	1.93	1.16	1.28	1.79	1.84	1.30	1.55	1.34	4.11
SLREE	30.2	48.1	96.9	101.2	103.6	119.1	137.6	115.7	138.8	131.1	117.9	100.1	78.4	100.1	150.6	164.5	136.0	164.8	128.9	243.9
SHREE	4.73	7.35	7.00	11.54	8.89	9.08	10.60	10.46	10.35	6.85	10.31	10.34	7.18	7.51	11.34	11.96	9.74	6.95	6.31	6.76

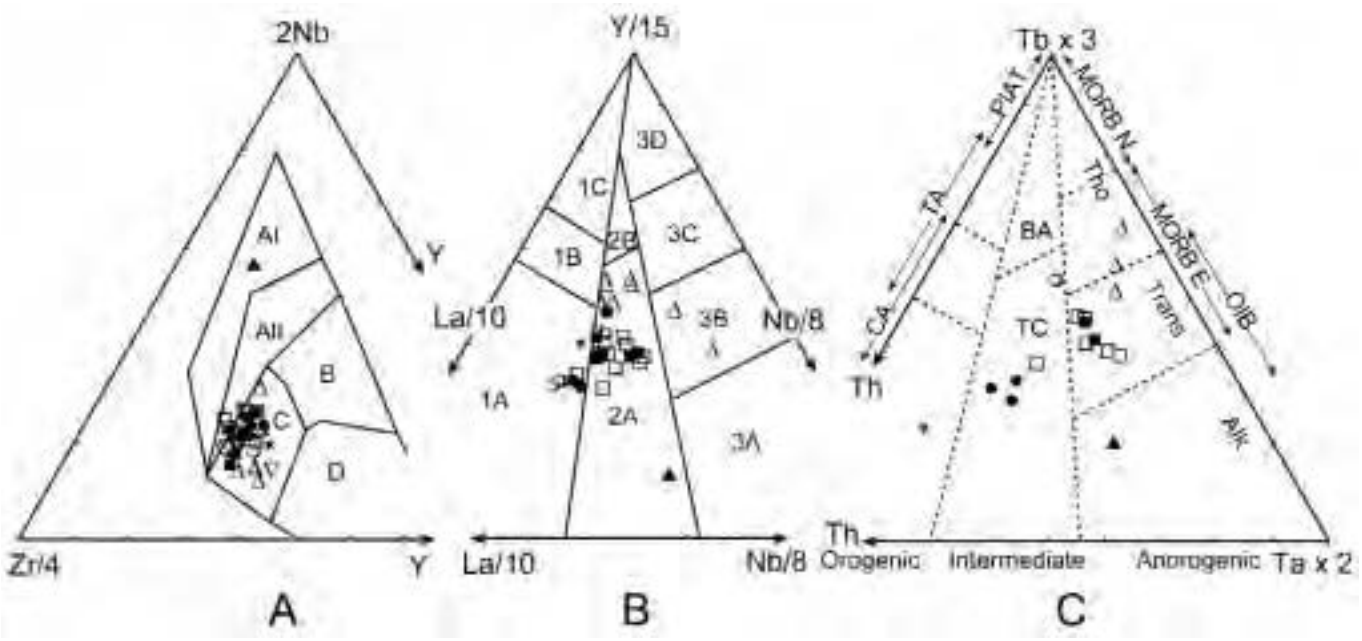

Fig. 9 - Geotectonic discrimination diagrams A): 2Nb-Zr/4-Y diagram (Meschede, 1986). Fields: AI- within-plate alkali basalts; AII- within-plate alkali basalts and within-plate tholeiites; B- E-type MORB; C- within-plate tholeiites and volcanic-arc basalts; D- N-type MORB and volcanic-arc basalts. B): La/10-Y/15-Nb/8 diagram (Cabanis and Lecolle, 1989). Fields: 1A- calc-alkali basalts; 1C- volcanic-arc tholeiites; 1B- area of overlap between 1A and 1C; 2A- continental basalts; 2B- back-arc basin basalts; 3A- alkali basalts from intercontinental rift; 3B, 3C- E-MORB; 3D- N-MORB. C): Th-3Tb-2Ta diagram (Cabanis and Thieblemont, 1988). Abbreviations: CA- calc-alkaline basalts, TA- arc-tholeiites; PIAT- primitive island arc tholeiites; Tho- N-MORB and, more rarely, E-MORB; Trans- transitional basalts; Alk- ocean island (OIB) and continental alkali basalts; BA- fore-arc and immature back-arc basin basalts; TC- continental tholeiites. Symbols as in Fig. 5.

GEOCHRONOLOGIC CONSTRAINTS

Calc-alkaline and alkaline intrusives

$^{40}Ar/^{39}Ar$ plateau ages of biotite separated from intrusives cut by basic dikes are respectively 286.1±1.4 Ma, 286.5±4.3 Ma (Stazzo Sitagliaccio granodiorite), 292.1±1.0 Ma (Stazzo Piredda granodiorite) and 294.5±4.5 Ma (Coddu Vecchio diorite) (Table 6). The four total fusion ages are concordant with plateaus ages. In all cases the initial increment gives the youngest age and apparent ages increase of the first 5-10% gas released to approach the total fusion ages. The age spectra indicate homogeneous argon isotopic contents and imply that biotite was essentially closed to argon diffusion after cooling.

U-Pb dating of zircon from the Arzachena granite (Monte Tiana sub-unit) yielded 311+6/-4 Ma (CARG sheet n. 428, Arzachena). These results agree with recent U-Pb zircon ages obtained from ‘U2’ calc-alkaline granites and ‘U2’ basic magmatism and A-type plutons from the northern part of the Sardinia-Corsica batholith (Cocherie et al., 2005, Table 6).

Dolerite dikes

Two $^{40}Ar/^{39}Ar$ age determinations of dolerite dikes were carried out on amphibole separates from the basaltic trachyandesite LG51 and the trachybasalt LG52 (Conca Verde swarm). The separated fractions were analyzed with the $^{40}Ar/^{39}Ar$ incremental method. Sample LG51 is characterized by an age spectrum (Fig. 11A) with two intermediate plateaus. Age values range between 253.8±4.9 Ma and 204.7±5.3 Ma. In the Ca/K spectrum (not reported), points corresponding to the different plateaus were grouped according to two different ages and Ca/K values (3.4-8 and 20-24 respectively). Sample LG52 is characterized by a staircase age spectrum (Fig. 11B), nevertheless two intermediate plateaus could be determined: the first low temperature plateau is characterized by an age of 195.0±13.6 Ma, the second plateau has an age of 248.4±8.8 Ma. The Ca/K values also randomly rise with temperature. On the inverse isochrone diagrams of both samples, points corresponding to two different plateaus forme different linear trends characterized by age values concordant with weighted mean plateau ages. The second temperature step (253.8±4.9 Ma and 248.4±8.8 Ma) was probably the age of emplacement.

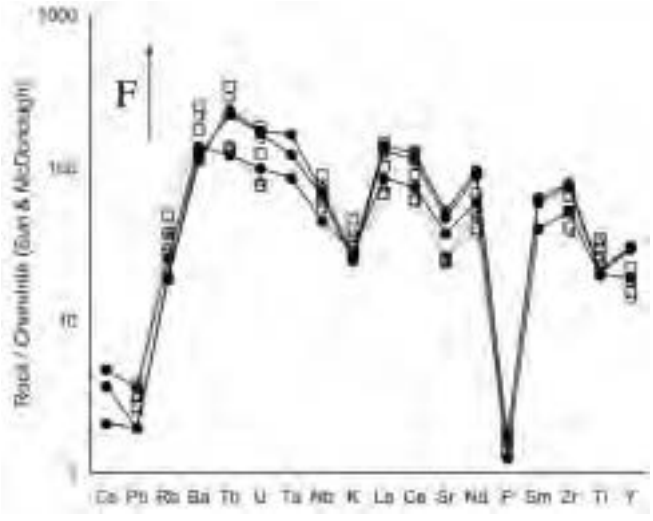

Fig. 10 - Chondrite-normalized spiderdiagram (after Sun and McDonough, 1989); calculation of AFC (De Paolo, 1981) from the most primitive basaltic magma at 0.2 (empty triangle), 0.4 (empty square) and 0.6 (empty circle) ratios of the rate of assimilation to the rate of crystallization (r), assuming AA39 monzogranite as contaminant. Represented fractions of magma remaining (F) are: 60% at 0.2 r, 60-70-80% at 0.4 r and 80-90% at 0.6 r. The Conca Verde dike is reported for comparison (filled circle).

Probably the temperature step corresponding to 204.7±5.3 Ma is probably related to recrystallization during a sub-greenschist overprint.

Lamprophyre dike

The data obtained by Baldelli et al. (1987) from biotite and amphibole extracted from the lamprophyre were analyzed with the K/Ar method. The ages obtained were 214.5±10.7 Ma and 227.6±3.0 Ma respectively. The authors consider the older age value on the amphibole more reliable due to the lower analytical error in the measurement. The fission track method carried out on apatite and biotite (Baldelli et al., 1987) yielded the following ages: 229±10 Ma, 240±11 Ma, 235±13 Ma, 227±15 Ma on apatite and 245±20 Ma, 247±20 Ma, 224±16 Ma on biotite (Table 6).

Nd - Sr ISOTOPIC COMPOSITION

The measured $^{87}Sr/^{86}Sr$ and $^{143}Nd/^{144}Nd$ ratios range between 0.70526±0.00004 ÷ 0.70787±0.00004 and 0.512529±0.000025 ÷ 0.513143±0.000023, respectively (Table 7). The Nd and Sr isotope ratios were corrected back to 254 Ma ($^{40}Ar/^{39}Ar$ dating of amphibole, present work), and the data are shown in Fig.12A as epsilon notation. The initial ε_{Nd} values range between -0.1 (sample LG 127) and +10.8 (sample LG 33), suggesting that these magmas range from strongly depleted in character to bulk Earth values. The Nd model ages calculated on a depleted source range between 0.5 and 0.9 Ga, and the ε_{Nd} value of the initial ratio ranges between +7.0 and + 5.9, suggesting a depleted character of the mantle source.

It is remarkable that the Sr isotopic composition is decoupled from the Nd isotope ratio, since all the studied samples (and sample LG 108 to a lesser extent) are shifted towards an exceedingly high radiogenic ^{87}Sr content with respect to the Mantle Array. Higher values of the $^{87}Sr/^{86}Sr$ ratios may result from 1) contamination of the magma with radiogenic ^{87}Sr derived from the continental crust, 2) selective Sr enrichment in the mantle source due to fluid circulation inducing metasomatism, 3) enrichment processes due to secondary alteration.

As a whole, the isotopic data variability suggests lithospheric mantle sources characterized by remnants of variably depleted materials.

In the Ba/Yb (not reported) and Ba/Y vs. $^{87}Sr/^{86}Sr$ correlation diagrams (Fig.12B), transitional dikes mirror the enriched mantle sources vector trend. The St. Pantaleo and Penisola Coluccia dikes are shifted toward a high $^{87}Sr/^{86}Sr$

Table 6 - Geochronologic data. Present work data are shown in bold letters.

Lithology	Sardinia			Corsica
	NE Sardinia		E-SE Sardinia	
A-type intrusives				
Quartz-syenites				
Leucomonzogranites				
Granites				
Calc-alkaline intrusives				
Granites	**286.1±1.4 and 286.5±4.3 Ma (Hb)** Stazzo Sbaghiascio	**292.1±1.0 Ma (Bt)** Stazzo Pirulida	**294.5±4.5 Ma (Bt)** Cedda Veychia	
Granodiorites				
Diorites				
Gabbroic complex				
Gabbros				
Calc-alkaline dykes				
Basaltic andesites and andesites			289±9 Ma (1) 291±3 - 271±8 Ma (1) 286±5 Ma (1)	
Dacites				287±3 Ma (1)
Basaltic dykes				
Trachybasalts and basanites	**253.8±4.9 Ma (Hbl)** **248.4±8.8 Ma (Hbl)** Conca Verde			
Trachyandesites				
Transitional basalts				
Alkali-basalts		114.5±1.0 / 113±7.20 Ma (2) 270±10 Ma (2)		

Italic characters indicate literature data: (1) Traversa et al. (2003) and references within; (2) Baldelli et al. (1987); (3) Cocherie et al. (2005) and references within.

Table 7 - Isotopic composition of Sr and Nd. t = assumed age on the basis of $^{39}Ar/^{40}Ar$ dating of the Conca Verde dike.

Provenance	Lithology	Sample	Symbol	t (Ma)	$^{87}Rb/^{86}Sr$	$^{87}Sr/^{86}Sr$	$(^{87}Sr/^{86}Sr)_i$	e $(Sr)_i$	$^{147}Sm/^{144}Nd$	$^{143}Nd/^{144}Nd$	e $(Nd)_i$
S.Pantaleo	sub-alkalic basalt	LG33	Δ	254	0,4922	0.70715 ± 3	0,705371	+16,56	0,1673	0.513143 ± 23	+10,81
Palau	transitional basalt	LG108	Δ	254	0,2982	0.70526 ± 4	0,704183	-0,32	0,1470	0.512827 ± 24	+5,30
Mirialveda	transitional basalt	LG38	□	254	0,3387	0.70635 ± 3	0,705126	+13,08	0,1477	0.512838 ± 24	+5,50
Costa Serena	transitional basalt	LG101	□	254	0,3684	0.70710 ± 3	0,705769	+22,21			
Penisola Coluccia	transitional basalt	LG127	□	254	0,3227	0.70787 ± 4	0,706704	+35,49	0,1339	0.512529 ± 25	-0,09

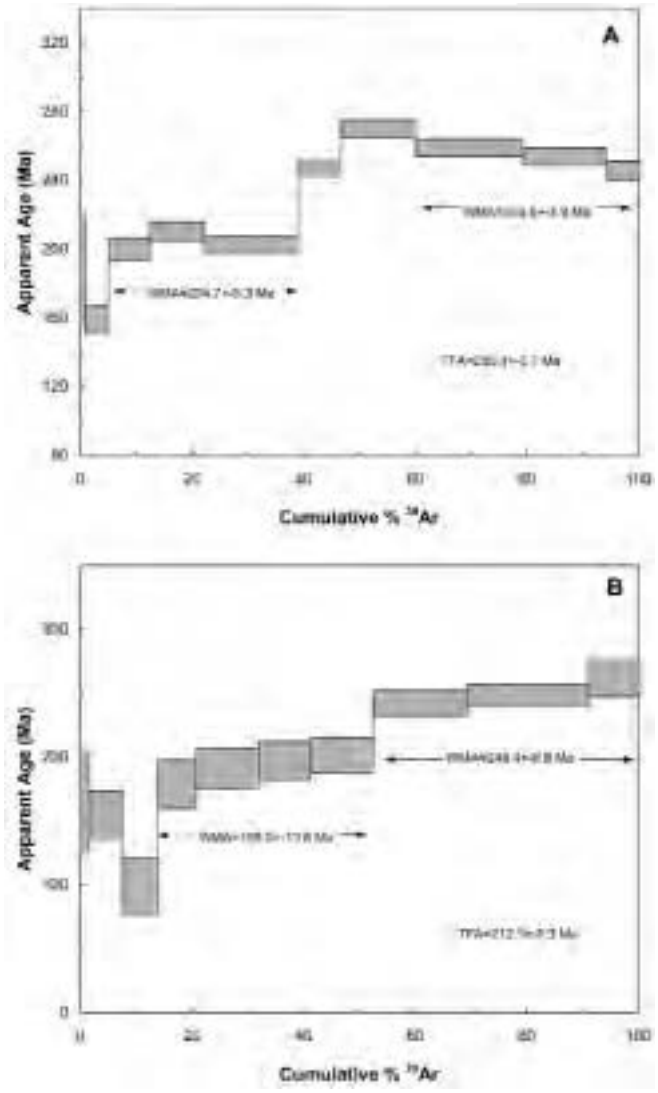

Fig. 11 - Apparent age spectrum $^{40}Ar/^{39}Ar$ for amphibole fractions separated by A) sample LG51; B) sample LG52.

isotopic ratio and suggest a remarkable contribution of crustal components, in accordance with the petrographic evidence of granite assimilation (biotite-quartz-plagioclase inclusions), mostly occurring at the chilled margins, as suggested by the $eNd_{(i)}$ vs. Ti/Yb x 10^{-4} diagram (Fig.12C).

DISCUSSION

Chemical composition and source region

A cogenetic relationship among the Sardinia doleritic dikes was revealed, for example, by the Mg# variation diagrams of major and trace elements. The composition confirms the evidence for low-pressure crystal fractionation through olivine, plagioclase and pyroxene precipitation. In dolerites, the presence of olivine phenocrysts and biotite inclusions in clinopyroxene supports silica undersaturation during the first stage of crystallization, evolving toward saturation. The CIPW classification as olivine - hyperstene - diopside normative basalts and the alkali content intermediate between subalkaline and alkaline series are consistent with a transitional affinity. Low Mg# values (29-50), relatively high SiO_2 (43.56 to 51.69 wt%) and high LILE contents typical of continental flood basalts, suggest a within-plate geodynamic setting. It is evident that the most primitive dolerite dikes (low Mg# values and Cr, Ni and Sr contents) do not correspond to a primary magma in equilibrium with mantle minerals, in particular the high Zr contents (average = 239 ppm) suggest evolved compositions of basaltic liquids or a Zr-enriched source.

A marked Nb and Ta negative anomaly in MORB-normalized spiderdiagrams characterizes many continental flood basalts, similar to, although less pronounced than that displayed by subduction-related magmas (Wilson, 1991). The Nb and Ta trough in within-plate basalts is interpreted as related to: 1) an "orogenic" component, perhaps a hydrous metasomatized mantle that preserves a record of older subduction events (Cabanis and Thiéblemont, 1988; Cabanis et al., 1990); 2) the involvement of lower continental crust in the mantle source (Innocent et al., 1994) or some segments of the continental lithospheric mantle (Hooper and Hawkesworth, 1993 and references within). More difficult to detect, 3) the existence of a residual Nb and Ta-bearing phase during the partial melting process (Wilson, 1991), however, the Sardinian dolerite shows only a marked negative Nb anomaly. The lack of negative Ta anomalies and low Th/Ta ratios characterizes anorogenic basalts, and is also typical of many transitional and tholeiitic basalts associated with incipient rifting events (Cabanis et al., 1990; Leroy and Cabanis, 1993).

The Conca Verde and Penisola Coluccia dolerites however show variable Si, Al, K and Na contents probably from assimilation of granitic host rocks, as supported by petrography and Sr isotopic data (e.g. for Penisola Coluccia). The La/Nb ratio of the Sardinian dolerite dikes (between 0.5 and 3.1), assumed to be a crustal contamination index (Thompson et al., 1984), overlaps the range of continental basalts (0.5-7) and is significantly higher for the Montiferru di Tertenia, Calangianus, Penisola Coluccia and Conca Verde dikes. The Mt. Nieddu lamprophyre has a La/Nb ratio = 0.9, consistent with alkaline continental basalts (< 1). The Th/Ta (Fig. 13) indicates crustal contamination from the most primitive to the evolved dolerites, and a predominant crystal fractionation trend within the subgroup of intermediate dolerites; an enriched mantle source and an active continental margin setting are delineated for the lamprophyre. Granite assimilation can account for LREE and LILE enrichments at least for the Conca Verde and Penisola Coluccia dikes; in particular, the LREE fractionation could indicate different extents of assimilation.

For the studied dolerites, the horizontal array extending to high values of $^{87}Sr/^{86}Sr$, can be interpreted as a mixing process of depleted and enriched end-members, i.e. EM II-type compositions within the sub-continental source mantle. Assimilation of Sr-rich crust by Sr-depleted, evolved magmas due to plagioclase fractionation (Wörner et al., 1986) is less probable. In fact, the Th/Ta confirms that the most primitive magma originated in a depleted mantle source (Fig. 12). The data set points to different depleted mantle sources with a variably time-integrated, depleted to almost undifferentiated, character, as the depleted mantle model yields 0.5 and 0.9 Ga ages for transitional dolerites, the latter likely representing the crustal extraction phase.

The observed Nd isotopic variability could represent: 1) kilometer scale heterogeneity (Kellogg et al., 2002; Meibom and Anderson, 2003) in a source mantle with homogeneous solidus temperature; 2) partial melting of a mantle portion with relatively fertile zones having lower solidus temperatures than the surrounding depleted matrix; 3) solid-state mixing of the uprising plumes during their ascent within a

large vertical section of mantle (Zindler and Hart, 1986). Besides these plausible petrogenetic mechanisms, and taking into account the association of the transitional igneous activity with the on-going lithospheric stretching within the Pangea, the extensive time span suggested by the depleted mantle model age (T_{DM} 0.5-0.9) probably records a melt extraction at progressively increasing depths in continuity with the model of Ferré and Leake (2001) and Paquette et al. (2003) for the early Carboniferous activity in Corsica.

Regional scenario and petrogenetic features

Dikes and flows ascribed to the early post-Variscan igneous cycle are known from different regions of the southern Variscan belt, such as Morocco (Aït Chayeb et al., 1998), the Pyrenees (Debon and Zimmermann, 1993; Deroin and Bonin, 2003), the Southalpine Domain (Cassinis et al., 2007), Sardinia (Traversa et al., 2003), and the Western Carpathians (Dostal et al., 2003) and are particularly abundant in Provence (Lapierre et al., 1999; Leroy and Cabanis, 1993) and Corsica (Traversa et al., 2003).

The Permo-Triassic (275-235 Ma, Broutin et al., 1994) tholeiitic transitional series from Provence, that includes basalt sills and dolerites of the Esterel, the Agay Basin basalts and the trachytes of Batterie des Lions (Lapierre et al., 1999), shows significant geochemical similarities with the Sardinia dolerite dikes, in spite of some Cr depletion and Ni enrichment. The thick mid-Permian (Toutin, 1980) basaltic lavas of Toulon (Leroy and Cabanis, 1993), are classified as transitional tholeiites for their REE abundance close to that of St. Pantaleo, with slight HREE fractionation in the primitive terms, and with significant La and Ce enrichment in the more evolved terms.

Alkalic-transitional to alkalic basaltic necks and dikes of the Western High Atlas (Aït Chayeb et al., 1998) and dike swarms of the western Pyrenean axial zone (Debon and Zimmermann, 1993) are characterized by fractionated REE patterns and the absence of negative Nb anomalies.

The tholeiitic basalts of Anayet (the Pyrenees) and La Rhune (the Basque Country) (Cabanis and Le Fur Balouet, 1990) show remarkable geochemical similarities to the tholeiitic transitional series in Provence (Leroy and Cabanis, 1993) and to the dolerites of the present study. The presence of negative Ta anomalies has been related with a late-orogenic calc-alkaline component to the source for Esterel, Corsica and the Basque Country basalts, whereas the Ta content of Toulon, the Anayet basalts and the late intrusions in Esterel and Corsica are related either to a late orogenic, or to off-axis emplacement with respect to the core of the orogen, where the Lower Permian calc-alkaline volcanic cycle developed (Leroy and Cabanis, 1993).

In the Southalpine domain, Triassic tholeiitic-transitional basalts from Val Cavallina (Cassinis et al., 2007) have REE abundances comparable with those of St. Pantaleo, with slight LREE fractionation (La_N/Sm_N = 1.92), a slightly lower HFSE content, and prominent positive K spikes in MORB-normalized spiderdiagrams. In the Central Western Carpathians (Slovakia) mafic lava flows and subordinate dikes and volcaniclastites of the Autunian-Saxonian-Thuringian (i.e. 299-251 Ma, http://www.chronos.org/) Maluzina Fm. have tholeiitic affinity (Dostal et al., 2003), close to that of the Sardinian dolerite dikes.

On the whole, the present work evidences the temporal overlap between alkaline activity and the transitional dolerite dikes, their emplacement spanning between ≈ 290

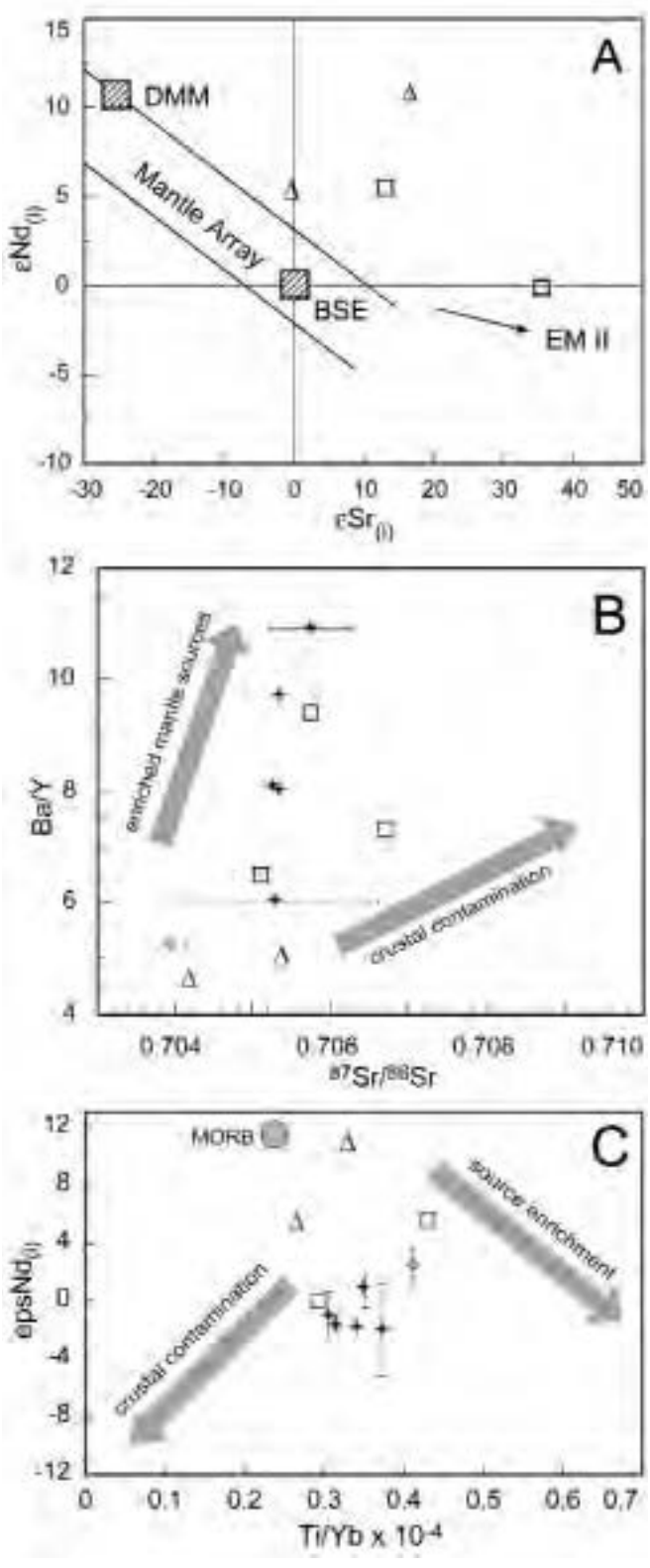

Fig. 12 - A) εNd vs εSr correlation diagram, symbols as in Fig. 5. DMM and EMII are approximations of mantle end-members members taken from Zindler and Hart (1986). B) Ba/Y-$^{87}Sr/^{86}Sr$ correlation diagram. C) Initial εNd - Ti/Yb x 10^{-4} correlation diagram. MORB field taken from Wilson, 1991. For comparison are reported the average $^{87}Sr/^{86}Sr$ isotopic ratios, εNd and trace element ratios of tholeiitic, transitional, lati-basalts (bold cross) and mildly alkaline basalt (cross) dikes from Sardinia and Corsica (Traversa et al., 2003). Error bar indicates the range of initial $^{87}Sr/^{86}Sr$ isotopic ratios and εNd.

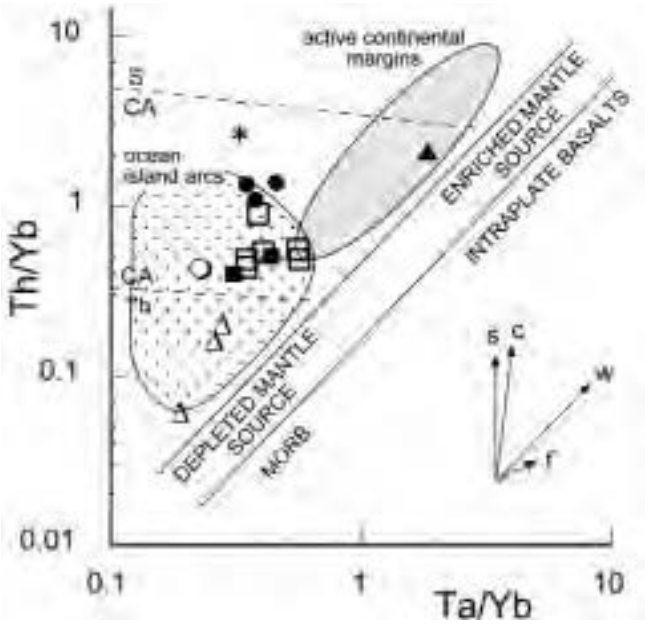

Fig. 13 - Th/Yb vs. Ta/Yb diagram (after Pearce, 1983). Vectors indicate the subduction components (s), within-plate enrichment (w), crustal contamination (C) and fractional crystallization (f). Dashed lines separate the tholeiitic (Th), calc-alkaline (CA), and shoshonitic (S) fields. Symbols as in Fig. 5.

(Traversa et al., 2003 and reference within) and ≈ 250 Ma (this work). The petrogenesis and the age of the dolerites have thus a bearing on the transition between the late phases of Variscan orogenesis and the Triassic rifting of the Pangea. Muttoni et al., (2003) has envisaged the stepwise evolution of lower Permian Pangea B to the Upper Permian Pangea A, suggesting a mid Permian stage of transformation after the cooling of the Variscan basement, and the strike slip tectonics that generated the Collio-type basins in the Southern Alps. The transformation would have been favored by the crustal weakness related to igneous activity along the Variscan suture. The key area for this evolution is indicated in the Southern Alps for the apparent igneous and sedimentary record preserved (Cassinis et al., 2007 and references therein; Schaltegger and Brack, 2007). In comparison, the Sardinia (and Corsica) settings can be defined as igneous-dominated both at depth and at the surface. The transitional dolerites could represent magmas issued from partial melting of lithospheric subcontinental mantle since the intermediate phases of the Variscan collapse, that encompassed residence in the lower and intermediate crust, thus allowing various extents of contamination. The tectonic unroofing of the Variscan chain accompanied and followed by delamination of the continental lithosphere, could have triggered partial melting of the lithospheric mantle at depth. In this phase the conspicuous crustal melting should have occurred due to the rise of asthenospheric mantle to accommodate erosion and consequent decompression of the continental roots. The emplacement of transitional dolerite dikes suggest that between 290 and 250 Ma a progressive tapping to magmatic reservoirs occurred, likely favored by the crustal delamination active at regional scale. The dikes would thus record the tectonic switch from crustal-dominated to deeper magmatism, elsewhere recorded as a sedimentary gap. A dynamic scenario characterized Sardinia (and Corsica) in the Middle and Late Permian, before the tectonic and magmatic transition related to the Neotethyan rift that produced the Triassic alkaline basalts.

CONCLUDING REMARKS

- A continental within-plate geochemical signature, with prevalent tholeiitic to transitional terms and a few alkalic dike, is recognized in Sardinia. Crustal contamination variably affects some (e.g. Conca Verde, Penisola Coluccia) of the dikes with transitional features; the host Arzachena monzogranite is the most probable contaminant source.
- The relative LILE and REE enrichment compared with the MORBs and Nd isotopic ratios can be consistent with a source in a sub-continental lithospheric mantle. The remarkable compositional and isotopic variability can be ascribed to the partial melting of a heterogeneous source, followed by crustal contamination of melts originating in a relatively poorly enriched source and by crystal fractionation.
- In Sardinia, the age of the alkaline dikes is significantly younger than that of the late Variscan alkaline volcanites and dikes of the Mediterranean domain (e.g. Eastern Provence: 278-264 Ma, $^{40}Ar/^{39}Ar$ isotope dating on feldspar from rhyolites and on plagioclase from a mafic flow, Zheng et al., 1992; Western Pyrenean Axial Zone: 271-266 Ma, K-Ar isotope dating on kaersutite phenocrysts from mafic dikes, Debon and Zimmermann, 1993); however calc-alkaline and peraluminous dikes in Sardinia were dated between 259 (Rb-Sr on biotite, Ronca et al., 1999) and 291 Ma (Rb-Sr on biotite, Vaccaro et al., 1991), consistent with the diachronism of the post-orogenic and anorogenic igneous activities in different areas of the Mediterranean domain (Traversa et al., 2003; Debon and Zimmermann, 1993).
- A chronological overlap results between the “post-orogenic” and “anorogenic” Permian igneous activities in the Sardinian-Corsican batholith. The overlap between the plutonic and volcanic calc-alkaline event and the volcanic and sub-volcanic alkalic event is not exclusive to Sardinia and Corsica, as such an abrupt compositional variation has been recognized in other collisional domains (Debon and Zimmermann, 1993; e.g. the Pyrenees and the Pan-African orogen, Adrar des Iforas).
- A widespread, largely coeval igneous event can be envisaged, on a geochemical basis, between the Sardinian dolerite dikes and the volcanic rocks ascribed to the Permian tholeiitic-transitional series (e.g Provence, Western Carpathia).
- The “anorogenic” Permian (Early and Late) magmatic activity results indipendent from the oncoming Neo-Tethyan rift. Only the Upper Triassic alkaline basalt of Mt. Nieddu can be definitely ascribed to a rifted crust.
- On the whole, the emplacement of transitional dolerites between ≈ 290 and 250 Ma could represent the evidence for the propagation of lithospheric delamination, and tapping of mantle-derived, crust-contaminated, magmatic reservoirs. In a pre-drift restoration the N-S emplacement trend coincides with the patterns of extension between the European and Insubric crusts at the onset of the Tethyan rift. The dolerites would therefore represent the evidence, elsewhere lacking (e.g. Liguria, Southern Alps) of crustal thinning and lithospheric wrenching over a transcurrent front some thousands km long.

ACKNOWLEDGEMENTS

The authors wish to thank G.P. Cherchi and A. Aversano (Progemisa S.p.A.), managers of the CARG sheet n. 428, Arzachena and n. 411, Bocche di Bonifacio survey project, for assistance in the field work.

REFERENCES

Aït Chayeb E.H., Youbi N., El-Boukhari A., Bouabdelli M. and Amrhar M., 1998. Le volcanisme permien et mésozoïque inférieur du bassin d'Argana (Haut-Atlas occidentale, Maroc): un magmatisme intraplaque associé à l'overture de l'Atlantique central. J. Afr. Earth Sci., 26: 499-519.

Baldelli C., Bigazzi G., Elter F.M. and Macera P., 1987. Description of a permo-trias alkaline lamprophyre embedded into the micaschists of garnet-staurolite-kyanite grade of North-eastern Sardinia island. F.P. Sassi and R. Bourrouilh (Eds.), IGCP n°5 Newsletter, 7: 7-10.

Bodinier J.L., Burg J.P., Leyreloup A. and Vidal H., 1988. Réliques d'un bassin d'arc subducté puis obducté dans la région de Marvejols (Massif Central). Bull. Soc. Géol. France, 8: 21-33.

Bonin B., 1989. Permian volcanosedimentary events in Corsica: a geological record of a waning Variscan Orogenesis and its transition to divergent plate boundary processes. Rend. Soc. Geol. It., 12: 139-141.

Bonin B., Brändlein P., Bussy F., Desmons J., Eggenberger U., Finger F., Graf K., Marro Ch., Mercolli I., Oberhänsli R., Ploquin A., von Quadt A., von Raumer J.F., Schaltegger U., Steyrer H.P., Visonà D. and Vivier G., 1993. Late Variscan magmatic evolution of the Alpine basement. In: J.F. von Raumer and F. Neubauer (Eds.), Pre-Mesozoic geology in the Alps. Springer-Verlag, p. 171-201.

Bouchardon J.-L., Santallier D., Briand B., Ménot R.-P. and Piboule M., 1989. Eclogites in the French Palaeozoic Orogen: geodynamic significance. Tectonophysics, 169: 317-322.

Briand B., Piboule M. and Bouchardon J.L., 1988. Diversité géochimique des metabasites des Groupes Leptyno-Amphiboliques du Rouergue et de Marvejols (Massif Central): origine et implications. Bull. Soc. Géol. France, 8 (4): 489-498.

Broutin J., Cabanis B., Chateauneuf J.J. and Deroin J.P., 1994. Biostratigraphy, magmatism, and tectonics of the SW European realm during the Permian times with paleogeographic consequences. Bull. Soc. Géol. France, 165 (2): 163-179.

Cabanis B., Cochemé J.J., Vellutini P.J., Joron J.L. and Treuil M., 1990. Post-collisional Permian volcanism in northwestern Corsica: an assessment based on mineralogy and trace-element geochemistry. J. Volcan. Geoth. Res., 44: 51-67.

Cabanis B. and Lecolle M., 1989. Le diagramme La/10-Y/15-Nb/8: un outil pour la discrimination des séries volcaniques et la mise en evidence des processus de mélange et/ou de contamination crustale. C. R. Acad. Sci., Ser. II, 309: 2023-2029.

Cabanis B. and Le Fur Balouet S., 1990. Le magmatisme crétacé des Pyrénées - Apport a la géochimie des éléments en traces - conséquences chronologiques et géodynamiques. Bull. Centres Rech. Explor.-Prod. Elf-Aquitaine, 14:155-184.

Cabanis B. and Thieblemont D., 1988. La discrimination des tholeiites continentales et des basaltes arrière-arc - Proposition d'un nouveau diagramme, le triangle Th-Tbx3-Tax2. Bull. Soc. Géol. France, 4 (6): 927-935.

Cappelli B., Carmignani L., Castorina F., Di Pisa A., Oggiano G. and Petrini R., 1991. A Variscan suture zone in Sardinia: geological and geochemical evidence. Geodin. Acta, 1: 101-118.

CARG sheet N. 411 - Bocche di Bonifacio 2006. Note Illustrative. In progress.

CARG sheet N. 428 - Arzachena 2006. Note Illustrative. In progress.

CARG sheet N. 549 - Muravera 2001. Note Illustrative. Servizio Geologico d'Italia. Regione Autonoma Sardegna.

Carmignani L., Carosi R., Di Pisa A., Gattiglio M., Musumeci G., Oggiano G. and Pertusati P.C., 1994. The hercynian chain in Sardinia (Italy). Geodin. Acta, 7 (1): 31-47.

Cassinis G., Cortesogno L., Gaggero L., Perotti C.R. and Buzzi L., 2006. Permian to Triassic geodynamic and magmatic evolution of the Brescian Prealps (Eastern Lombardy, Italy), submitted.

Cassinis G., Cortesogno L., Gaggero L., Perotti C.R. and Ronchi A. 2007 Volcanic products from the Early Permian Collio Basin (Southern Alps) and their geodynamic implications. Per. Mineral., 76 (2), in press.

Cassinis G., Cortesogno L., Gaggero L., Ronchi A., Sarria E., Serri R. and Calzia P., 2003. Reconstruction of igneous, tectonic and sedimentary events in the latest Carboniferous - Early Permian Seui Basin (Sardinia, Italy), and evolutionary model. Boll. Soc. Geol. It., Vol. Spec., 2: 99-117.

Cassinis G., Cortesogno L., Gaggero L., Ronchi A. and Valloni R., 1996. Stratigraphic and petrographic investigations into the Permian-Triassic continental sequences of Nurra (NW Sardinia). Quad. Geol. Iberica, 21: 149-169.

Cocherie A., Rossi P., Fanning C.M. and Guerrot C., 2005. Comparative use of TIMS and SHRIMP for U-Pb zircon dating of A-type granites and mafic tholeiitic layered complexes and dikes from the Corsican Batholith (France). Lithos, 82: 185-219.

Cortesogno L., Cassinis G., Dallagiovanna G., Gaggero L., Oggiano G., Ronchi A., Seno S. and Vanossi M., 1998. The Variscan post-collisional volcanism in Late Carboniferous-Permian sequences of Ligurian Alps, Southern Alps and Sardinia (Italy): a synthesis. Lithos, 45: 305-328.

Cortesogno L., Dallagiovanna G., Gaggero L. and Vanossi M., 1993. Elements of the Palaeozoic History of the Ligurian Alps. In: J.F. von Raumer and F. Neubauer (Eds.), Pre-Mesozoic geology in the Alps. Springer-Verlag, p. 257-277.

Cortesogno L., Gaggero L., Oggiano G. and Paquette J.L., 2004. Different tectono-thermal evolutionary path in eclogitic rocks from the axial zone of the Variscan Chain in Sardinia (Italy) compared with the Ligurian Alps. Ofioliti, 29: 125-144.

Curnelle R. and Cabanis B., 1989. Relations entre le magmatisme «triasique» et le volcanisme infra-liasique des Pyrénées et de l'Aquitaine - Apports de la géochimie des éléments en trace - Conséquences chronologiques et géodynamiques. Bull. Centres Rech. Explor.-Prod. Elf-Aquitaine, 13: 347-376.

Debon F. and Zimmermann J.L., 1993. Mafic dikes from some plutons of the western Pyrenean Axial Zone (France, Spain): markers of the transition from late-Hercynian to early-Alpine events. Schweiz. Mineral. Petrogr. Mitt., 73: 421-433.

DePaolo D.J., 1981. Trace element and isotopic effects of combined wallrock assimilation and fractional crystallization. Earth Planet. Sci. Lett., 53: 189-202.

Deroin J.P. and Bonin B., 2003. Late Variscan tectonomagmatic activity in Western Europe and surrounding areas: the Mid-Permian episode. Boll. Soc. Geol. It., Vol. Spec., 2: 169-184.

Dostal J., Vozàr J., Keppie J.D. and Hovorka D., 2003. Permian volcanism in the Central Western Carpathians (Slovakia): Basin-and-range type rifting in the southern Laurussian margin. Intern. J. Earth Sci., 92: 27-35.

Ferré E.C. and Leake B.E., 2001. Geodynamic significance of early orogenic high-K crustal and mantle melts: example of the Corsica Batholith. Lithos, 59: 47-67.

Gebauer D., Williams I.S., Compston W. and Grunenfelder M., 1988. Archean zircons in a retrograded, Caledonian eclogite of the Gotthard Massif (Central Alps, Switzerland). Schweiz. Mineral. Petrogr. Mitt., 68: 485-490.

Gradstein F.M., Ogg J.G., Smith A.G., Agterberg F.P., Bleeker W., Cooper R.A., Davydov V., Gibbard P., Hinnov L.A., House M.R., Lourens L., Luterbacher H.P., McArthur J., Melchin M.J., Robb L.J., Shergold J., Villeneuve M., Wardlaw B.R., Ali J., Brinkhuis H., Hilgen F.J., Hooker J., Howarth R.J., Knoll A.H., Laskar J., Monechi S., Plumb K.A., Powell J., Raffi I., Röhl U., Sadler P., Sanfilippo A., Schmitz B., Shackleton N.J., Shields G.A., Strauss H., Van Dam J., Van Kolfschoten T.,

Veizer J., Wilson D., 2004. A geologic time scale 2004. Cambridge Univ. Press, 589 pp.

Green T.H., 1982. Anatexis of mafic crust and high pressure crystallization of andesite. In: R.S. Thorpe (Ed.), Andesites. John Wiley and Sons. Ltd., p. 465-487.

Hooper P.R. and Hawkesworth C.J., 1993. Isotopic and geochemical constraints on the origin and evolution of the Columbia River Basalt, Journal of Petrology, 34: 1203-1246.

Innocent C., Briqueu L. and Cabanis B., 1994. Sr-Nd isotope and trace element geochemistry of late Variscan volcanism in the Pyrenees: magmatism in post-orogenic extension? Tectonophysics, 238: 161-181.

Kellogg J.B., Jacobsen S.B. and O'Connel R.J., 2002. Modeling the distribution of isotopic ratios in geochemical reservoirs, Earth Planetary Science Letters, 204: 183-202.

Komar P.D., 1972. Flow differentiation in igneous dikes and sills: profiles of velocity and phenocryst concentration. Geol. Soc. Am. Bull., 83: 3443-8.

Laird J. and Albee A.L., 1981. Pressure, temperature, and time indicators in mafic schists: their application to reconstructing the polymetamorphic history of Vermont. Am. J. Sci., 281: 127-175.

Lapierre H., Basile C. and Dupuis V., 1999. Basaltes et trachytes permiens de l'Estérel (SE France): une serie tholéiitique transitionnelle épanchée pendant l'amincissement lithosphérique. Bull. Soc. Géol. France, 170: 253-265.

Leake B. E., Woolley A.R., Arps C.E.S., Birch W.D., Gilbert M.C., Grice J.D., Hawthorne F.C., Kato A., Kisch H.J., Krivovichev V.G., Linthout K., Laird J., Mandarino J.A., Maresch W.V., Nickel E.H., Rock N.M.S., Schumacher J.C., Smith D.C., Stephenson N.C.N., Ungaretti L., Whittaker E.J.W. and Youzhi G., 1997. Nomenclature of amphiboles: report of the subcommittee on amphiboles of the International Mineralogical Association, Commission on new minerals and mineral names, Canad. Mineral., 35: 219-246.

Leroy S. and Cabanis B., 1993. Le volcanisme permien du bassin de Toulon: un jalon septentrional du vulcanisme permien de l'Ovest méditerranéen. Géol. France, 2: 57-66.

Liégeois J.P. and Duchesne J.C., 1981. The Lac Cornu retrograde eclogites (Aiguilles Rouges Massif, Western Alps, France): evidence of crustal origin and metasomatic alteration. Lithos, 14: 35-48.

Ludwig K.R., 1994. Analyst. A computer program for control of a thermal-ionization single-collector mass-spectometer. U. S. Geol. Survey Open-file Rep., 92-543.

Macera P., Conticelli S., Del Moro A., Di Pisa A., Oggiano G. and Squadrone A., 1989. Geochemistry and Rb-Sr age of syntectonic peraluminous granites of Western Gallura, Northern Sardinia: constraints on their genesis. Per. Mineral., 58: 25-43.

Meibom A. and Anderson D.L., 2003. The statistical upper mantle assemblage. Earth Planet. Sci. Lett., 217: 123-139.

Ménot R.-P. and Paquette J.L., 1993. Geodynamic significance of basic and bimodal magmatism in the external domain. In: J.F. von Raumer and F. Neubauer (Eds.), Pre-Mesozoic geology in the Alps. Springer-Verlag, Berlin, p. 241-254.

Meschede M., 1986. A method of discriminating between different types of mid-ocean ridge basalts and continental tholeiites with the Nb-Zr-Y diagram. Chem. Geol., 56: 207-218.

Morimoto N., Fabries J., Ferguson A.K., Ginzburg I.V., Ross M., Seifert F.A., Zussman J., Aoki K. and Gottardi G., 1988. Nomenclature of pyroxenes. Am. Mineral., 73: 1123-1133.

Muñoz M., Coujault-Radé P. and Tollon F., 1992. The massive stibnite veins of the French Paleozoic basement: a metallogenic marker of Late Variscan brittle extension. Terra Nova, 4: 171-177.

Muttoni G, Kent D. V., Garzanti E. Brack P., Abrahamsen N. and Gaetani M., 2003. Early Permian Pangea 'B' to Late Permian Pangea 'A'. Earth Planet. Sci. Lett., 215: 379-394

Nakamura N., 1974. Determination of REE, Ba, Fe, Mg, Na, and K in carbonaceous and ordinary chondrites. Geochim. Cosmochim. Acta, 38: 757-775.

Navidad M. and Alvaro M., 1985. El vulcanismo alcalino del Triasico Superior de Mallorca (Mediterraneo Occidental). Bol. Geol. Minero, 96 (1): 10-22.

Oggiano G., 1994. Lineamenti stratigrafico strutturali del basamento del Goceano (Sardegna centro settentrionale). Boll. Soc. Geol. It., 113: 105-115.

Paquette J.L., Ménot R.-P. and Peucat J.J., 1989. REE, Sm-Nd and U-Pb zircon study of eclogites from the Alpine External Massifs 'Western Alps): Evidence for crustal contamination. Earth Planet. Sci. Lett., 96: 181-198.

Paquette J.-L., Menot R.-P., Pin C. and Orsini J.-B., 2003. Episodic and short-lived granitic pulses in a post-collisional setting: evidence from precise U-Pb zircon dating through a crustal cross-section in Corsica, Chem. Geol., 198: 1-20.

Pearce J.A., 1983. The role of sub-continental lithosphere in magma genesis at destructive plate margins. In: C.J. Hawkesworth and M.J. Norry (Eds.), Continental basalts and mantle xenoliths. Shiva, Nantwich, p. 230-249.

Pearce J.A. and Parkinson I.J., 1993. Magmatic processes and plate tectonics, Geol. Soc. London Spec. Publ., 76: 373-403.

Pittau P., Barca S., Cocherie A., Del Rio M., Fanning M. and Rossi P., 2002. The Permian basin of Guardia Pisano (SW Sardinia, Italy): palynostratigraphy, paleophytogeography, correlations and radiometric age. Geobios, 35 (5): 561-580.

Poli G. and Tommasini S., 1999. Insights on acid-basic magma interaction from the Sardinia-Corsica batholith: the case study of Sarrabus, southeastern Sardinia, Italy. Lithos, 46: 553-571.

Rieder M., Cavazzini G., D'Yakonov Y.S., Frank-Kamenetskii V.A., Gottardi G., Guggenheim S., Koval, P.V., Muller G., Neiva A.M.R., Radoslovich E.W., Robert J.-L., Sassi F.P., Weiss Z. and Wones D.R., 1998. Nomenclature of micas. Canad. Mineral., 36: 41-48.

Rivalenti G., Garruti G., Rossi A., Siena F. and Sinigoi S., 1980. Existence of different peridotite types and of a layered igneous complex in the Ivrea zone of Western Alps. J. Petrol., 22: 127-153.

Rock N.M.S., 1990. The International Mineralogical Association (IMA/CNMMN) Pyroxene nomenclature scheme: Computerization and its consequences. Mineral. Petrol., 43: 211-227.

Ronca S., Del Moro A. and Traversa G., 1999. Geochronology, Sr - Nd isotope geochemistry and petrology of late - Hercynian dyke magmatism from Sarrabus (SE Sardinia). Per. Mineral., 68: 231-260.

Rossi P., Cocherie A., Fanning C.M. and Deloule E., 2006. Variscan to eo-Alpine events recorded in European lower-crust zircons sampled from the French Massif Central and Corsica, France. Lithos, 87: 235-260.

Rottura A., Del Moro A., Caggianelli A., Bargossi G.M. and Gasparotto G., 1997. Petrogenesis of the Monte Croce granitoids in the context of Permian magmatism in the Southern Alps, Italy. Eur. J. Mineral., 9: 1293-1310.

Schaltegger U. and Brack P., 2007. Crustal-scale magmatic systems during intracontinental strike-slip tectonics: U, Pb and Hf isotopic constraints from Permian magmatic rocks of the Southern Alps. Intern. J. Earth Sci., DOI: 10.1007/s00531-006-0165-8.

Sinigoi S., Quick J.E., Mayer A. and Demarchi G., 1995. Density-controlled assimilation of underplated crust, Ivrea-Verbano zone, Italy. Earth Planet. Sci. Lett., 129: 183-191.

Stähle V., Frenzel G., Hess J.C., Saupé F., Schmidt S.T. and Schneider W., 2001. Permian metabasalt and Triassic alkaline dikes in the northern Ivrea zone: clues to the post-Variscan geodynamic evolution of the Southern Alps. Schweiz. Mineral. Petrogr. Mitt., 81: 1-21.

Stenger R., Baatz K., Klein H. and Wimmenauer W., 1989. Metamorphic evolution of the pre-Hercynian basement of the Schwarzwald (Federal Republic of Germany). Tectonophysics, 157: 117-121.

Sun S.S., 1980. Lead isotopic study of young volcanic rocks from mid-ocean ridge, ocean islands and island arcs. Phil. Trans. R. Soc., A297: 409-445.

Sun S.S. and McDonough W.F., 1989. Chemical and isotopic systematics of oceanic basalts: implications for mantle composition and processes. In: A.D. Saunders and M.J. Norry (Eds.), Magmatism in ocean basins. Geol. Soc. London Spec. Publ., 42: 313-345.

Taylor S.R. and McLennan S.M., 1981. The composition and evolution of the continental crust: rare earth element evidence from sedimentary rocks. Phil. Trans. R. Soc., A301: 381-399.

Thompson R.N., Morrison M.A., Hendry G.L. and Parry S.J., 1984. An assessment of the relative roles of crust and mantle in magma genesis: an elemental approach. Phil. Trans. R. Soc., A310: 549-590.

Toutin N. 1980. Le Permien continental de la Provence orientale (France). Doct. Sci. Thesis, Nice Univ., 2 Vol., 594 pp.

Traversa G., Ronca S., Del Moro A., Pasquali C., Buraglini N. and Barabino G., 2003. Late to post-Hercynian dike activity in the Sardinia-Corsica Domain: A transition from orogenic calc-alkaline to anorogenic alkaline magmatism. Boll. Soc. Geol. It., Vol. Spec., 2: 131-152.

Traversa G. and Vaccaro C. 1992. REE distribution in the late Hercynian dikes from Sardinia. IGCP n. 276, Newsletter, 5: 241-262.

Vaccaro C., Atzori P., Del Moro A., Oddone N., Traversa G. and Villa I.M., 1991. Geochronology and Sr isotope geochemistry of late - Hercynian dikes from Sardinia. Schweiz. Mineral. Petrogr. Mitt., 71: 221-220.

Vatin-Perignon N. and Lemoine M., 1982. Volcanisme et sedimentation triasiques dans le Massif du Pelvoux (Alpes occidentales externes). Implication géodynamiques. C. R. Acad. Sci., Sci. Terre, 25: 159-173.

von Raumer J.F., Galetti G., Oberhansli R. and Pfeifer H.R., 1990. Amphibolites from Lac Emosson/Aiguilles Rouges (Switzerland): tholeiitic basalts at a transition zone between continental and oceanic crust. Schweiz. Mineral. Petrogr. Mitt., 70: 419-435.

Wilson M., 1991. Igneous petrogenesis a global tectonic approach. Harper Collins Acad., London, p. 287-323.

Winchester J.A. and Floyd P.A., 1977. Geochemical discrimination of different magma series and their differentiation products using immobile elements. Chem. Geol., 20: 325-343.

Wörner G., Zindler A., Staudigel H. and Schmincke H.-V., 1986. Sr, Nd, and Pb isotope geochemistry of Tertiary and Quaternary alkaline volcanics from West Germany. Earth Planet. Sci. Lett., 75: 37-49.

Zheng J.S., Mermet J.F., Toutin-Morin N., Hanes J., Gondolo R., Morin R. and Féraud G., 1992. Datation $^{40}Ar/^{39}Ar$ du magmatisme et de filons minéralisés permiens en Provence orientale (France). Geodin. Acta 5 (3): 203-215.

Ziegler P.A., Cloetingh S., Guiraud R. and Stampfli G.M., 2001. Peritethyan platforms: constraints on dynamics of rifting and basin inversion. In: P.A. Ziegler, W. Cavazza and A.H.F. Robertson (Eds.), Peritethyan rift/wrench basins and passive margins, Mem. Mus. Nat. Hist. Nat. Paris, 186: 9-49.

Ziegler, P.A. and Stampfli, G.M., 2001, Late Palaeozoic-Early Mesozoic plate boundary reorganization: collapse of the Variscan orogen and opening of Neotethys. In: G. Cassinis (Ed.), Permian continental deposits of Europe and other areas. Regional reports and correlations. “Natura Bresciana”, Ann. Mus. Civico Sci. Nat. Brescia, Monogr., 25: 17-34.

Zindler A. and Hart S., 1986. Chemical geodynamics, Ann. Rev. Earth Planet. Sci., 14: 493-571.

Received, September 18, 2006
Accepted, May 25, 2007